



**HAL**  
open science

## **RISE controller tuning and system identification through machine learning for human lower limb rehabilitation via neuromuscular electrical stimulation**

Héber H. Arcolezi, Willian R.B.M. Nunes, Rafael A. de Araujo, Selene Cerna,  
Marcelo A.A. Sanches, Marcelo C.M. Teixeira, Aparecido de Carvalho

### ► **To cite this version:**

Héber H. Arcolezi, Willian R.B.M. Nunes, Rafael A. de Araujo, Selene Cerna, Marcelo A.A. Sanches, et al.. RISE controller tuning and system identification through machine learning for human lower limb rehabilitation via neuromuscular electrical stimulation. *Engineering Applications of Artificial Intelligence*, 2021, 102, pp.104294. 10.1016/j.engappai.2021.104294 . hal-03739559

**HAL Id: hal-03739559**

**<https://hal.science/hal-03739559>**

Submitted on 27 Jul 2022

**HAL** is a multi-disciplinary open access archive for the deposit and dissemination of scientific research documents, whether they are published or not. The documents may come from teaching and research institutions in France or abroad, or from public or private research centers.

L'archive ouverte pluridisciplinaire **HAL**, est destinée au dépôt et à la diffusion de documents scientifiques de niveau recherche, publiés ou non, émanant des établissements d'enseignement et de recherche français ou étrangers, des laboratoires publics ou privés.

# RISE Controller Tuning and System Identification Through Machine Learning for Human Lower Limb Rehabilitation via Neuromuscular Electrical Stimulation

Héber H. Arcolezi<sup>a,b,\*</sup>, Willian R. B. M. Nunes<sup>c</sup>, Rafael A. de Araujo<sup>b</sup>, Selene Cerna<sup>a</sup>, Marcelo A. A. Sanches<sup>b</sup>, Marcelo C. M. Teixeira<sup>b</sup>, Aparecido A. de Carvalho<sup>b</sup>

<sup>a</sup>*Femto-ST Institute, Univ. Bourgogne Franche-Comté, UBFC, CNRS, Belfort, 90000, France*

<sup>b</sup>*Department of Electrical Engineering, São Paulo State University, UNESP, Ilha Solteira, 15385-000, Brazil*

<sup>c</sup>*Department of Electrical Engineering, Federal University of Technology - Paraná, UTFPR, Apucarana, 86812-460, Brazil*

---

## Abstract

Neuromuscular electrical stimulation (NMES) has been effectively applied in many rehabilitation treatments of individuals with spinal cord injury (SCI). In this context, we introduce a novel, robust, and intelligent control-based methodology to closed-loop NMES systems. Our approach utilizes a robust control law to guarantee system stability and machine learning tools to optimize both the controller parameters and system identification. Regarding the latter, we introduce the use of past rehabilitation data to build more realistic data-driven identified models. Furthermore, we apply the proposed methodology for the rehabilitation of lower limbs using a control technique named the robust integral of the sign of the error (RISE), an offline improved genetic algorithm optimizer, and neural network models. Although in the literature, the RISE controller presented good results on healthy subjects, without any fine-tuning method, a

---

\*Corresponding author

*Email addresses:* [heber.hwang\\_arcolezi@univ-fcomte.fr](mailto:heber.hwang_arcolezi@univ-fcomte.fr) (Héber H. Arcolezi), [willianr@utfpr.edu.br](mailto:willianr@utfpr.edu.br) (Willian R. B. M. Nunes), [rafael.araujo@unesp.br](mailto:rafael.araujo@unesp.br) (Rafael A. de Araujo), [selene\\_leya.cerna\\_nahuis@univ-fcomte.fr](mailto:selene_leya.cerna_nahuis@univ-fcomte.fr) (Selene Cerna), [marcelo.sanches@unesp.br](mailto:marcelo.sanches@unesp.br) (Marcelo A. A. Sanches), [marcelo.minhoto@unesp.br](mailto:marcelo.minhoto@unesp.br) (Marcelo C. M. Teixeira), [aa.carvalho@unesp.br](mailto:aa.carvalho@unesp.br) (Aparecido A. de Carvalho)

trial and error approach would quickly lead to muscle fatigue for individuals with SCI. In this paper, for the first time, the RISE controller is evaluated with two paraplegic subjects in one stimulation session and with seven healthy individuals in at least two and at most five sessions. The results showed that the proposed approach provided a better control performance than empirical tuning, which can avoid premature fatigue on NMES-based clinical procedures.

*Keywords:* Neuromuscular electrical stimulation, Spinal cord injury, RISE controller, Knee joint, Machine learning.

---

## 1. Introduction

Neuromuscular electrical stimulation (NMES) and functional electrical stimulation (FES) have been effectively applied in many rehabilitation treatments for people with spinal cord injury (SCI) in the past years. Damages in the spinal cord may be engendered by traumatic causes such as road accidents, sports injuries, and violence, or nontraumatic ones such as diseases and tumors. Spinal cord injury is commonly a permanent cause, which can generate issues such as loss of bodily perception, difficulties related to sexual functions, partial or total paralysis, and severe pain (Ho et al. (2014); Lynch & Popovic (2008); Popović (2014); Wagner et al. (2018)). However, the main consequences depend on several factors, such as the patient's personal condition, the level of the lesion and its damages, the availability of time and resources, and socioeconomic factors. For instance, in low-income countries, SCI normally leads to death, whereas in high-income countries, people with SCI enjoy a better and more productive life (Bickenbach (2013)).

The application of NMES/FES for SCI rehabilitation is one of the most frequently used methods (Marquez-Chin & Popovic (2020); Kapadia et al. (2020)). It provides many health and social benefits to patients; for example, it helps to preserve and recover muscle strength and prevent flaccidity and hypotrophy, which are evidence of muscle inactivity; it also offers higher expectation and quality of life, and facilitates social reinsertion (Peckham & Knutson

22 (2005); Marquez-Chin & Popovic (2020); Lynch & Popovic (2008)). Moreover,  
23 NMES/FES are techniques based on the use of equipment that generates elec-  
24 trical signals for muscle stimulation at the motor level. More specifically, the  
25 aim is generating a muscle contraction via electrodes placed superficially or in-  
26 tramuscularly. The electrical stimulation consists of applying a pulsed current  
27 or voltage signal that can depolarize neurons above the activation threshold.  
28 The amplitude, pulse width (PW), frequency, and shape of the pulse determine  
29 which neurons are recruited. Muscle control can be realized by amplitude, PW,  
30 or frequency modulation (Lynch & Popovic (2012); Popović (2014)).

31 Even though there are several investigations on the closed-loop control of  
32 NMES/FES systems for lower limb rehabilitation (*cf.* Ferrarin et al. (2001);  
33 Previdi & Carpanzano (2003); Jezernik et al. (2004); Cheng et al. (2016); Mo-  
34 hammed et al. (2012); Wu et al. (2017); Hmed et al. (2017); Sharma et al. (2012);  
35 Gaino et al. (2017); dos Santos et al. (2015); Nunes et al. (2019); Teodoro et al.  
36 (2020); Müller et al. (2017); Page & Freeman (2020); Gaino et al. (2020) and the  
37 references within), these systems are hardly put into production. Alternatively,  
38 there exist commercial stimulators normally available on open-loop designs and  
39 with pre-programmed electrical stimulation, which are not adequate to deal  
40 with the nonlinear and time-varying nature of muscles (Page & Freeman (2020);  
41 Lynch & Popovic (2012)). Hence, given the numerous challenges in the design  
42 of automatic stimulation strategies, further investigation is needed in this field.  
43 For example, control strategies are needed to compensate for modeling errors on  
44 the plant, system faults, individual’s muscles behavior, and inter/intra-subject  
45 variability in muscle properties (Sharma et al. (2009, 2012); Yu et al. (2013,  
46 2015)). The variability in muscle properties leads to the difficulty of predicting  
47 the exact contraction force exerted by the muscle, which results in unknown  
48 mapping between the stimulation parameters and the muscle force.

49 In this sense, the design and evaluation of the robust integral of the sign of  
50 the error (RISE) control (Xian et al. (2003); Xian et al. (2004)) for tracking the  
51 nonlinear dynamics of electrically stimulated lower limbs are presented in this  
52 paper. Despite several control laws investigated in the literature, this study

53 considers RISE control law by some fundamental characteristics, such as the  
54 consideration of unmodeled disturbances and uncertainties in the plant. Never-  
55 theless, adjusting the controller parameters is the main component to guarantee  
56 high-quality control performance; that is, the method can only guarantee good  
57 responses (semi-global asymptotic stability), appropriately selecting the gain  
58 constants.

59 Stegath et al. (2007, 2008) and Sharma et al. (2009) are pioneers authors  
60 on RISE controller development for the lower limb tracking control. After-  
61 ward, Sharma et al. (2012) presented an improvement of RISE control method  
62 for the same application using a feedforward neural network (NN) term. Downey  
63 et al. (2013) and Downey et al. (2015) developed an RISE controller for the asyn-  
64 chronous stimulation to the lower limb. Kawai et al. (2014) simulated the track-  
65 ing control performance of an RISE-based controller to model the co-contraction  
66 control of the human lower limb. Kushima et al. (2015) modeled an FES knee  
67 bending and stretching system, and developed an RISE-based controller to stim-  
68 ulate the quadriceps and hamstring muscle groups. In the similar context of  
69 NMES, but for upper limbs, Lew et al. (2016) implemented RISE controller for  
70 the rehabilitation of post-stroke individuals.

71 Even though previous investigations for this problem with RISE controller  
72 presented good results without any fine-tuning method, the motivation of this  
73 paper is the absence of clever algorithms to properly select the gain constants  
74 of RISE controller. In the aforementioned studies, the authors did not show the  
75 controller tuning method or empirical approach (pretrial tests) for defining gain  
76 parameters before the real experiments are conducted. In addition, experiment  
77 validations were made only on healthy individuals; however, the muscles of  
78 people with SCI are not as strong as healthy muscles (Mohammed et al. (2012);  
79 Lynch & Popovic (2012)).

80 More specifically, Stegath et al. (2008), Sharma et al. (2009), and Downey  
81 et al. (2015) present four inequalities to gain constants, which are sufficient con-  
82 ditions to guarantee semi-global asymptotic stability for an uncertain nonlinear  
83 muscle model. There are infinite combinations of gains in  $\mathbb{R}^+$  that satisfy these

84 inequalities; yet, as presented in the aforementioned works, a “trial and error”  
85 methodology might be feasible to set gain constants to the controller for healthy  
86 subjects. However, this procedure must be reconsidered when treating people  
87 with SCI to avoid some common problems. For instance, for SCI rehabilitation  
88 via NMES/FES, there might exist rapid muscle fatigue, muscle tremors due  
89 to incomplete tetanus, and harsh muscle spasms (Ho et al. (2014); Lynch &  
90 Popovic (2012); Popović (2014); Peckham & Knutson (2005)).

91 Therefore, to overcome the aforementioned problems, this paper proposes a  
92 novel robust and intelligent control-based methodology for NMES/FES systems.  
93 More precisely, we aim to overcome the empirical tuning technique for clinical  
94 procedures using RISE controller, as observed in the literature. Moreover, this  
95 study proposes to extend the analysis of RISE controller to individuals with  
96 SCI that do not present ideal conditions as healthy individuals. The proposed  
97 methodology includes an identification step based on machine learning (ML)  
98 black-box models with the novelty of using past identification and control data  
99 for each patient, a robust control law (e.g., RISE technique) to guarantee the  
100 semi-global asymptotic stability, and an ML-based offline controller optimizer.

101 In Arcolezi et al. (2019), our group proposed an offline improved genetic  
102 algorithm (IGA) optimizer to RISE controller. Simulations were performed  
103 using a nonlinear mathematical model of the knee joint for three paraplegics and  
104 one healthy individual. In this study, our proposed methodology is implemented  
105 and evaluated with seven healthy and two paraplegic individuals using RISE  
106 control law, the aforementioned IGA optimizer, and NN black-box models.

107 The first hypothesis in this paper is that using an empirical approach to  
108 clinical procedures would present a large number of poor performances, while a  
109 more adequate tuning with a more representative identified model can provide  
110 better tracking control of the lower limb. That is, we assume no background  
111 knowledge with the RISE controller for clinicians intending to design and apply  
112 it to real-life scenarios. The second hypothesis is that by using past rehabilita-  
113 tion data for identifying an individual, this model will improve the description of  
114 the relationship between the angular position and the delivered electrical stim-

115 ulation, whereby fatigue and other problems as tremors are already implicit in  
 116 the data.

117 The remaining sections of this paper are organized as follows: Section 2  
 118 presents the theoretical background; Section 3 introduces the proposed control-  
 119 based methodology and the materials and methods used in the experiments;  
 120 Section 4 presents the results and its analysis; and finally, Section 5 provides  
 121 the conclusions of this paper and future works.

## 122 2. Theoretical Background

123 In this section, we briefly present the musculoskeletal dynamics about the  
 124 knee joint (Subsection 2.1) and RISE control method (Subsection 2.2). We  
 125 summarize the IGA for the optimization procedure (Subsection 2.3), and we  
 126 discuss nonlinear system identification via NN models (Subsection 2.4).

### 127 2.1. System dynamics

The musculoskeletal dynamics based on electrical stimulation is given as  
 (Ferrarin et al. (2001); Sharma et al. (2009))

$$J\ddot{\theta}(t) = \Lambda_g(\theta(t)) + \Lambda_e(\theta(t)) + \Lambda_v(\dot{\theta}(t)) + \Lambda_d(t) + \Lambda_{es}(t), \quad (1)$$

128 where  $J \in \mathbb{R}$  is the unknown inertia of the combined shank and foot;  
 129  $\theta(t)$ ,  $\dot{\theta}(t)$ ,  $\ddot{\theta}(t) \in \mathbb{R}$  is the angular position, velocity and acceleration, respec-  
 130 tively.

The gravitational component  $\Lambda_g(\theta(t)) \in \mathbb{R}$  is expressed as

$$\Lambda_g(\theta(t)) = -mgl \sin(\theta(t)), \quad (2)$$

131 where  $m \in \mathbb{R}$  denotes the unknown combined mass of the shank and foot;  $l \in \mathbb{R}$   
 132 is the unknown length between the knee-joint and center of mass of the shank  
 133 and foot; and  $g \in \mathbb{R}$  is the gravitational acceleration.

The elastic effects due to joint stiffness  $\Lambda_e(\theta(t)) \in \mathbb{R}$  can be modeled as

$$\Lambda_e(\theta(t)) = -(\psi_1\theta(t) - \psi_1\psi_3) \left( e^{-\psi_2\theta(t)} \right), \quad (3)$$

134 where  $\psi_1, \psi_2, \psi_3 \in \mathbb{R}$  are unknown positive coefficients.

The viscous effects due to damping  $\Lambda_v(\dot{\theta}(t)) \in \mathbb{R}$  is defined as

$$\Lambda_v(\dot{\theta}(t)) = -\kappa_1 \tanh(-\kappa_2 \dot{\theta}(t)) + \kappa_3 \dot{\theta}(t), \quad (4)$$

135 where  $\kappa_1, \kappa_2, \kappa_3 \in \mathbb{R}$  are unknown positive constants.

The torque produced at the knee joint by the electrical stimulation  $\Lambda_{es}(t) \in \mathbb{R}$  is related to the positive moment  $\varsigma(\theta(t)) \in \mathbb{R}$  from the extension and flexion of the leg, the unknown nonlinear function  $\nu(\theta, \dot{\theta}) \in \mathbb{R}$  corresponding to muscle tendon force, and the electrical potential  $u(t) \in \mathbb{R}$  applied to the quadriceps muscle:

$$\Lambda_{es}(t) = \varsigma(\theta(t))\nu(\theta(t), \dot{\theta}(t))u(t). \quad (5)$$

136 Finally,  $\Lambda_d(t) \in \mathbb{R}$  is the unmodeled bounded disturbances (e.g., fatigue,  
137 spasms, tremor, and delay).

## 138 2.2. RISE-based control

139 RISE control method proposed by Xian et al. (2003); Xian et al. (2004) uti-  
140 lizes a continuous and high gain control signal, which guarantees semi-global  
141 asymptotic stability considering bounded smooth external disturbances and  
142 bounded modeling uncertainties. The use of the integral of the sign of the  
143 error in RISE technique minimizes the commonly chattering problem seen in  
144 sliding-mode controllers. To achieve the stated control objective, i.e., to enable  
145 the lower limb to track a desired angular trajectory despite external disturbances  
146 and modeling uncertainties, a position tracking error denoted by  $e_1(t) \in \mathbb{R}$ , is  
147 defined as

$$e_1(t) = \theta_d(t) - \theta(t), \quad (6)$$

148 where  $\theta_d(t)$  is the angular trajectory to be tracked with the premise of having  
149 bounded continuous-time derivatives, and  $\theta(t)$  is the real angular position. Fur-  
150 thermore, to facilitate the control design, filtered tracking errors  $e_2(t) \in \mathbb{R}$  and



151  $r(t) \in \mathbb{R}$  are defined as

$$e_2(t) = \dot{e}_1(t) + \alpha_1 e_1(t), \quad (7)$$

$$r(t) = \dot{e}_2(t) + \alpha_2 e_2(t), \quad (8)$$

152 where  $\alpha_1, \alpha_2 \in \mathbb{R}$  are positive and selectable control gains.

Multiplying (8) by  $J$ , and considering (1)-(7),  $\dot{e}_2 = \ddot{\theta}_d(t) + \alpha_1 \dot{e}_1 - \ddot{\theta}(t)$ , one obtains

$$Jr = \Upsilon(\dot{\theta}_d, \dot{\theta}, \theta, \dot{e}_1, e_2) - \Psi(\dot{\theta}, \theta)u - \Lambda_d, \quad (9)$$

where  $\Upsilon(\dot{\theta}_d, \dot{\theta}, \theta, \dot{e}_1, e_2) \in \mathbb{R}$  defined as

$$\Upsilon(\dot{\theta}_d, \dot{\theta}, \theta, \dot{e}_1, e_2) = \ddot{\theta}_d + \alpha_1 \dot{e}_1 + \alpha_2 e_2 - \Lambda_g(\theta) - \Lambda_e(\theta) - \Lambda_v(\dot{\theta}),$$

and  $\Psi(\dot{\theta}, \theta) \in \mathbb{R}$  a function monotonic and bounded, expressed as

$$\Psi(\dot{\theta}, \theta) = \varsigma(\theta)\nu(\theta, \dot{\theta}).$$

153

For stability analysis, from (9) can be determined the open-loop error system

$$\mathcal{J}_\Psi r = \mathcal{Y}_\Psi - u - \mathcal{L}_\Psi,$$

where  $\mathcal{J}_\Psi = \Psi^{-1}J$ ,  $\mathcal{Y}_\Psi = \Psi^{-1}\Upsilon$ , and  $\mathcal{L}_\Psi = \Psi^{-1}\Lambda_d$ , and consequently one obtains

$$\mathcal{J}_\Psi \dot{r} = -\dot{u} - e_2 + \tilde{\mathcal{W}} + \mathcal{W}_d,$$

where  $\tilde{\mathcal{W}} = \mathcal{W} - \mathcal{W}_d$ ,  $\tilde{\mathcal{W}}(e_1, e_2, r, t) \in \mathbb{R}$ ,  $\mathcal{W} \in \mathbb{R}$  corresponds to the term

$$\mathcal{W} = -\frac{1}{2}\dot{\mathcal{J}}_\Psi r + \dot{\mathcal{Y}}_\Psi - \dot{\mathcal{L}}_\Psi + e_2,$$

and  $\mathcal{W}_d \in \mathbb{R}$  expressed as

$$\mathcal{W}_d = \dot{\mathcal{J}}_\Psi \ddot{\theta}_d + \mathcal{J}_\Psi \ddot{\theta}_d - \dot{\Lambda}_e - \dot{\Lambda}_g - \dot{\Lambda}_v - \dot{\Lambda}_d.$$

154

155 Based on the mean value theorem applied to upper bound  $\|\dot{\mathcal{W}}\| \leq$   
156  $\varsigma(\|\zeta\|)\|\zeta\|$ , where  $\zeta \in \mathbb{R}^3$ ,  $\zeta = [r^T e_1^T e_2^T]^T$ ,  $\varsigma(\|\zeta\|) \in \mathbb{R}$  is a positive globally  
157 invertible nondecreasing function, and considering that  $\theta_d$ , and its derivatives  
158  $\theta_d^{(k)} \in \mathcal{L}_\infty, \forall k \in \mathbb{I} = \{1, 2, 3, 4\}$ , the following constraints can be established  
159  $\|\mathcal{W}_d\| \leq \mathcal{E}_{\mathcal{W}_d}, \|\dot{\mathcal{W}}_d\| \leq \mathcal{E}_{\dot{\mathcal{W}}_d}$ , such as  $\mathcal{E}_{\mathcal{W}_d}, \mathcal{E}_{\dot{\mathcal{W}}_d} \in \mathbb{R}$  are positive constants (Utkin  
160 (2013)).

Note that the system error equations obtained to nonlinear dynamic model are similar to other studies with the RISE controller in (Sharma et al. (2009); Stegath et al. (2008); Patre et al. (2008); Makkar et al. (2007); Xian et al. (2004); Xian et al. (2003)). Based on the open-loop error system, the control input  $u(t) \in \mathbb{R}$ , is designed as

$$u(t) = (k_s + 1)e_2(t) - (k_s + 1)e_2(0) + \int_0^t [(k_s + 1)\alpha_2 e_2(\tau) + \beta \text{sgn}(e_2(\tau))] d\tau, \quad (10)$$

161 where  $k_s, \beta \in \mathbb{R}$  also represents positive and adjustable control gains,  $u(t)$  is the  
162 control signal, and  $\text{sgn}(\cdot)$  is the known signum function.

The RISE controller, given in (10), ensures that all system signals are bounded under closed-loop operation and the position tracking error is regulated in sense that

$$\lim_{t \rightarrow \infty} \|e_1(t)\| \rightarrow 0,$$

yields semi-global asymptotic stability provided the control gain  $k_s$  sufficiently large, and  $\beta$  satisfying the following sufficient condition

$$\beta > \mathcal{E}_{\mathcal{W}_d} + \frac{1}{\alpha_2} \mathcal{E}_{\dot{\mathcal{W}}_d}, \quad (11)$$

163 where  $\mathcal{E}_{\mathcal{W}_d}, \mathcal{E}_{\dot{\mathcal{W}}_d} \in \mathbb{R}$  are known positive constants. More details about the  
164 stability analysis of the RISE method can be found in (Patre et al. (2008);  
165 Makkar et al. (2007); Xian et al. (2004)).

The ideal first derivative of the error  $H(s) = \frac{Y(s)}{U(s)} = \frac{sE(s)}{E(s)} = s$  is an improper function, that is,  $H(s) = \frac{\sum_{j=0}^m b_j s^j}{\sum_{i=0}^n a_i s^i}$ ,  $a_i, b_j \in \mathbb{R}, \forall i = 1, 2, \dots, n, \forall j = 1, 2, \dots, m, m > n, |H(\infty)| = \infty$ . The unfeasibility of practical implementation using the ideal derivative is solved by a filtered derivative (Khadra

et al. (2016)). Thus, the filtered tracking error is calculated by

$$H(s) = \frac{Y(s)}{U(s)} = \frac{s}{\tau s + 1}, \quad (12)$$

166 where  $\tau$  is the time constant between the signal and its derivative. Note that (12)  
167 is a low pass filter (LPF) that attenuates high-frequency noises.

### 168 *2.3. Improved genetic algorithm*

169 The IGA was introduced in Arcolezi et al. (2019) to optimize the gains pa-  
170 rameters of RISE controller for a representative model of an individual. This  
171 algorithm is summarized in this paper. First, there is a pre-processing stage for  
172 bounding the gain limits to efficiently initiate (i.e., the random initial popula-  
173 tion within the constraints of stability) and maintain the search (i.e., genetic  
174 operators such as recombination, mutation, and replacement operator). Sec-  
175 ond, a simple fast genetic algorithm (FGA) is used in the construction phase  
176 to generate a good initial population. Thereafter, a complete genetic algorithm  
177 (CGA) is applied to improve the quality of this population and hence achieve a  
178 global (or local) minimum.

179 Figure 1 describes the FGA with a flow chart. In the chart,  $N_p$  is the size  
180 of the initial population (small),  $M_r$  is the mutation rate, and the stopping  
181 criterion is the number of generations  $N_g$ . More specifically,  $N_g$  represents the  
182 size of the real initial population (RIP) to initiate the local search phase. The  
183 CGA is similar to the FGA, with a more stringent test to the replacement  
184 operator. We recommend that readers refer to (Arcolezi et al. (2019)) for a  
185 more descriptive version of the algorithm.

### 186 *2.4. System identification via neural networks*

187 Nonlinear systems identification and modeling have been applied in most  
188 areas of science to predict the future behavior of dynamic systems. System  
189 identification has been an active field in control theory, and it is an important  
190 approach to explore, study, and understand the world by a formal description  
191 of events as a model. The use of NNs to identify nonlinear systems has been a

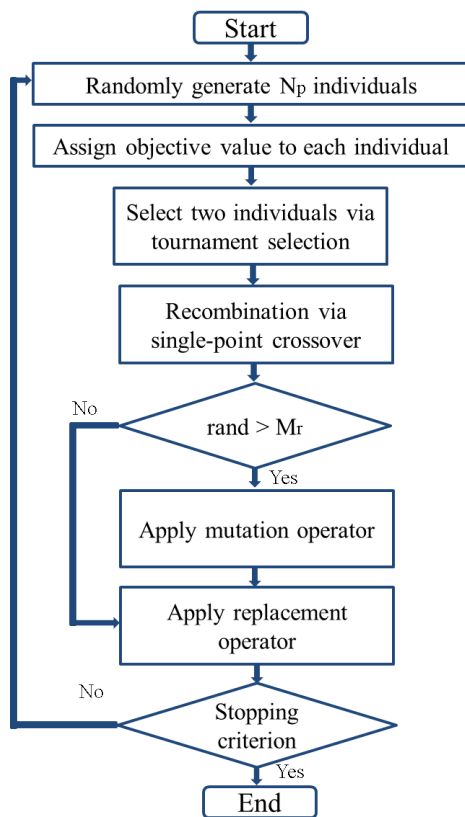


Figure 1: Flow chart of the fast genetic algorithm.

192 prospective direction since previous research presented in (Hornik et al. (1989);  
 193 Chen et al. (1990); Narendra & Parthasarathy (1990); Chu et al. (1990)), for  
 194 example. In the following, the use of NNs for the identification of discrete  
 195 dynamic system is briefly described.

196 The construction of black-box models is essentially based on the quality of  
 197 measured data about the system. The fundamental concept of this approach  
 198 is to model the direct input-output relationship, i.e., identifying and modeling  
 199 just with data, in which the main objective is to find the weights and other  
 200 coefficients (known as hyperparameters) of the NN. Moreover, NNs are based  
 201 on a collection of inter-connected units named neurons. These neurons are  
 202 structured into three or more layers, input, hidden(s), and output. Neural

203 networks are in the core of deep learning (several neurons and hidden layers)  
 204 and have become a progressively popular research topic. Generally, NNs can be  
 205 divided into two large classes: feedforward and recurrent NNs.

206 Fundamentally, an operator  $F$  from an input space  $\mathbb{U}$  to an output space  
 207  $\mathbb{Y}$  expresses the model of the system to be identified, where the goal is to find  
 208 a function  $\hat{F}$  that approximates  $F$  to a specific requirement. By the Stone-  
 209 Weierstrass theorem, there exists a continuous and bounded function  $F$ , that  
 210 can be uniformly approximated as closely as desired by a polynomial function  
 211  $\hat{F}$ . Furthermore, according to the universal approximation theorem, there exists  
 212 a combination of hyperparameters of an NN that allows it to identify and learn  
 213 any continuous nonlinear function defined on a closed interval (Hornik et al.  
 214 (1989)).

215 Consider a single-input and single-output discrete system structure with only  
 216 the input and output data available:

$$y(k) = F[y(k-1), \dots, y(k-n); u(k-1), \dots, u(k-m)], \quad (13)$$

217 where  $F(\cdot)$  is an unknown nonlinear difference equation that represents the plant  
 218 dynamics;  $u$  and  $y$  are measurable scalar input and output, respectively; and  $m$   
 219 and  $n$  are the maximum lags for the system output and input; that is, they are  
 220 the last values of the input and output respectively. In short, the next value of  
 221 the dependent output signal  $y(k)$  is regressed on previous values of the output  
 222 and input signals.

223 The identification for the discrete-time system in (13) can be performed  
 224 by the following two major types of identification structures presented in the  
 225 literature: the parallel and the series-parallel identification model (Narendra &  
 226 Parthasarathy (1990)). The first structure depends on past inputs of the system  
 227 and the outputs of the NN model. The second structure uses both past inputs  
 228 and system's outputs. Mathematically, these models are respectively described

$$\hat{y}(k) = \hat{F}[\hat{y}(k-1), \dots, \hat{y}(k-n); u(k-1), \dots, u(k-m)], \quad (14)$$

$$\hat{y}(k) = \hat{F}[y(k-1), \dots, y(k-n); u(k-1), \dots, u(k-m)], \quad (15)$$

230 where  $\hat{y}$  is the model output;  $y$  is the real system output;  $\hat{F}$  is the model  
 231 structure; and  $m$  and  $n$  are the regression orders for the input and output,  
 232 respectively. These last two parameters are chosen before the identification  
 233 process, where  $n$  is the output memory to indicate how many past steps of  
 234 output will be used in the system identification, and  $m$  refers to the time-step  
 235 of input values and it is the longest memory that a model can store. In this  
 236 paper, we used a feedforward NN (multilayer perceptron - MLP) to approximate  
 237 the nonlinear mapping function  $F(\cdot)$  in (13) using the series parallel structure  
 238 in (15).

### 239 3. Materials and Methods

240 In this section, we first present an overview of our proposed methodology  
 241 (Subsection 3.1). Next, we provide information on the volunteering participants  
 242 (Subsection 3.2) and on the instrumentation used for real experiments (Subsec-  
 243 tion 3.3). Lastly, we describe how we applied the proposed methodology in this  
 244 study for both, data acquisition and experimental procedures (Subsection 3.4).

#### 245 3.1. Proposed methodology

246 Fig. 2 illustrates an overview of the proposed methodology. In the first  
 247 session of a new patient (no previous data), a stimulation test is performed to  
 248 acquire information on the relationship between delivered electrical stimulation  
 249 and the achieved angular position. The acquired data are appropriately treated  
 250 to pass through an identification step via NN black-box models. Once this  
 251 relationship is efficiently mapped as a model, a simulation process is initiated  
 252 using clever algorithms. The aim is to minimize a well-defined objective function

253 to adequately set-up the gains of RISE controller for the patient. Therefore, to  
254 finalize the first session, the rehabilitation procedure is retaken with fine-tuned  
255 gains for a better control-stimulation session. This could prevent premature  
256 fatigue and other unwanted factors that would be present for people with SCI  
257 by not choosing an appropriate gain combination.

258 In future sessions, all data (system identification and control evaluation)  
259 from previous rehabilitation sessions are used for training an NN model in an  
260 offline scheme. That is, before each (next) session, all data from a patient are  
261 combined to a single dataset and used to map the relationship between angular  
262 position and electrical stimulation. Thus, the same optimization process using  
263 the trained model provides fine-tuned gain parameters to be afterward applied  
264 to the rehabilitation procedure. The gains of the controller are found using  
265 only past rehabilitation data, which is motivated by the belief that preliminary  
266 electrical stimulation could lead to quick muscle fatigue during the real clinical  
267 procedure. Moreover, between stimulation sessions, there exist factors such as  
268 fatigue, hydration, evolution/gain of strength, rest, and therapeutic sessions,  
269 which might influence one's response to NMES/FES and make the control-  
270 stimulation inefficiently.

271 The use of NNs is motivated by the advantages of these methods for the  
272 nonlinear system identification problem and by the high power for computation  
273 and storage of data encountered nowadays. Regarding the identification step,  
274 the novelty of the proposed methodology is the use of past rehabilitation data.  
275 The primary purpose is to build up a dataset for each patient, where the number  
276 of data will increase during rehabilitation sessions, and the identified model will  
277 improve with more data and details about the nonlinear muscular behavior.  
278 As highlighted in the literature, muscular behavior is susceptible to parametric  
279 variation between one day and another, for instance, the evolution and gain of  
280 strength due to previous rehabilitation sessions.

281 Moreover, one of the primary advantages of performing simulations for an  
282 NMES-based knee extension is the liberty of studying this problem from dif-  
283 ferent perspectives and divergent levels of abstraction with the acquired data.

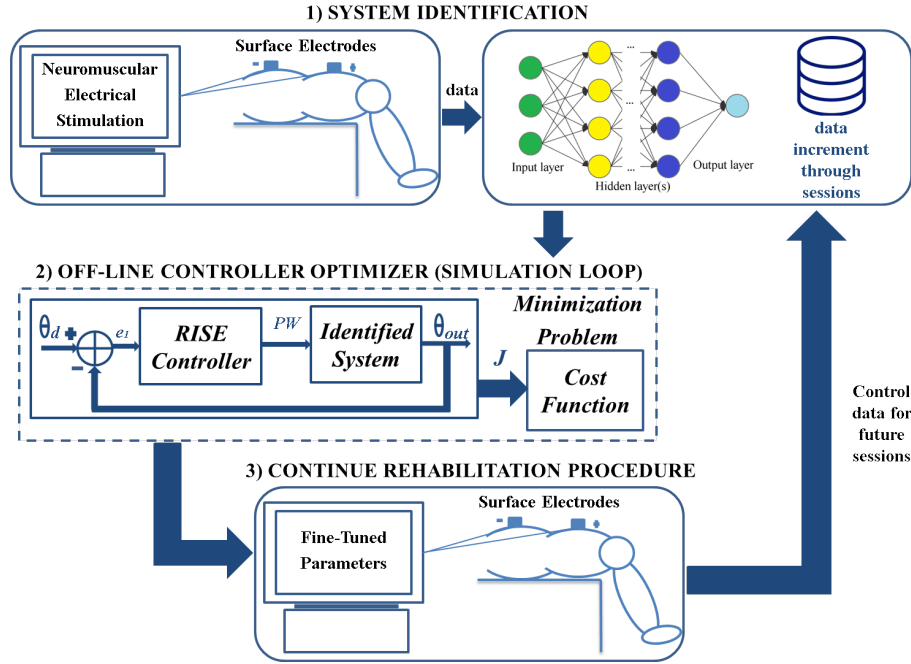


Figure 2: The proposed robust and intelligent control-based methodology.

284 While the application of NMES to humans presents limitations due to muscle fa-  
 285 tigue, which restricts the number of experiments, simulation provides numerous  
 286 executions to better study the feasibility and practicality of the designed system.  
 287 Moreover, simulation supplies continuous feedback to continuously improve the  
 288 system (Jezernik et al. (2004)).

### 289 3.2. Analyzed individuals

290 The study with volunteers was authorized through a research ethics commit-  
 291 tee involving human beings (CAAE: 79219317.2.1001.5402) at São Paulo State  
 292 University (UNESP). Written informed consent was obtained from all partici-  
 293 pants before their participation. In this study, seven healthy individuals (male,  
 294 aged 22-28) labeled as H1-H7 and two male individuals with SCI, labeled as P1  
 295 and P2, participated in the experiments. Table 1 presents information on the  
 296 two SCI individuals, including age, injury data, and ASIA (American Spinal  
 297 Injury Association) Impairment Scale (AIS).



Table 1: Specific data on individuals with SCI.

Individual	Age (years)	Injury level	Injury time	AIS
P1	32	L4, L5	9 years	B
P2	43	C5, C6	17 years	C

298 *3.3. Instrumentation*

299 Fig. 3 illustrates the test platform used for conducting the experiments at  
300 the Instrumentation and Biomedical Engineering Laboratory (“Laboratório de  
301 Instrumentação e Engenharia Biomédica - LIEB”) at UNESP - Ilha Solteira.  
302 The platform was composed of an NI (National Instruments<sup>®</sup>, USA) myRIO  
303 controller to operate in real time; a current-based neuromuscular electrical stim-  
304 ulator; an instrumented chair composed of an electrogoniometer NIP 01517.0001  
305 (Lynx<sup>®</sup>, São Paulo, Brazil), a gyroscope LPR510AL (ST Microelectronics<sup>®</sup>,  
306 Switzerland), two triaxial accelerometers MMA7341 (Freescale<sup>®</sup>, USA); and  
307 two user interfaces developed in LabVIEW<sup>®</sup>, one for identification and the  
308 other for controlling.

309 The neuromuscular electrical stimulator delivers rectangular, biphasic, sym-  
310 metrical pulses to the individual’s muscle, allowing a control adjustment of the  
311 PW in a range of 0 – 400 $\mu$ s. We controlled the stimulation intensity by setting  
312 the pulse amplitude to the quadriceps and controlling the PW. In this study,  
313 we fixed the following parameters: stimulation frequency at 25 Hz (constant  
314 frequency train - CFT technique) and pulse amplitude at 80 mA for healthy  
315 individuals and 120 mA for paraplegic ones. The difference in pulse amplitude  
316 occurred due to insufficient contractions using amplitude below 120 mA for the  
317 paraplegic individuals and their respective muscular atrophy conditions. Lastly,  
318 we used surface electrodes with rectangular self-adhesive CARCI 50 mm x 90  
319 mm settings.

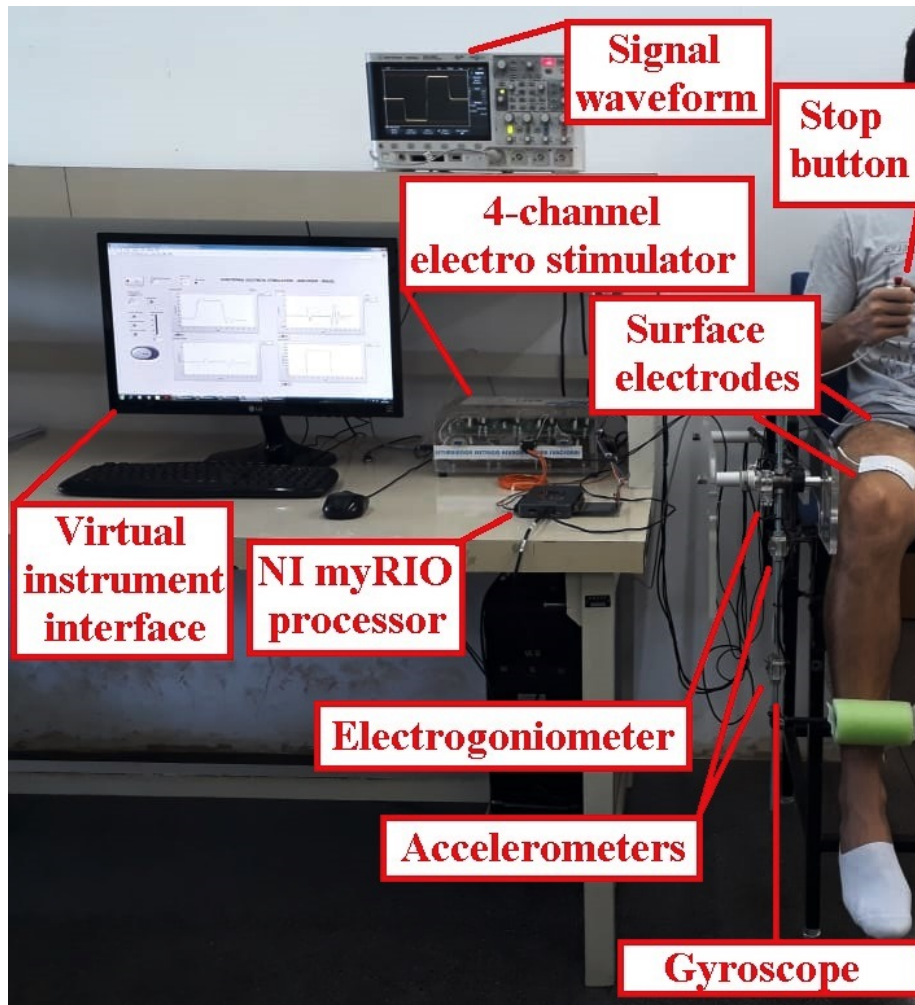


Figure 3: Test platform for electrical stimulation experiments.

320 *3.4. Data acquisition and experimental procedure*

321 The chair backrest and the knee joint position were adjusted to ensure the  
 322 volunteers' comfort. Each individual had a different knee angular position in  
 323 the resting condition. The angular position in this condition was measured and  
 324 taken as an offset during the experimental protocol. A muscle analysis was  
 325 conducted to determine the motor point and guarantee the proper positioning  
 326 of the surface electrodes. More precisely, the electrophysiological procedure

327 for identifying the motor point consists of mapping the muscle surface using a  
328 stimulation electrode to identify the skin area above the muscle, where the motor  
329 threshold is the lowest for a given electrical current; this skin area is the most  
330 responsive to electrical stimulation (Gobbo et al. (2014)). After this procedure,  
331 the electrodes were properly positioned allowing the neuromuscular electrical  
332 stimulation to maximize the effectiveness of the evoked voltage, minimizing the  
333 intensity of the injected current and the level of discomfort to the volunteer.

334 After the motor-point identification, a few open-loop tests were performed  
335 by applying a step input during four seconds. It is worth highlighting the  
336 definition of the electrical current level of the stimulator, as well as evaluating  
337 the PW values for different operating points of the lower limb extension. If the  
338 value  $\rho_{max}$  tends to the saturation value of the stimulator, the electrical current  
339 amplitude must be increased so that the control system adequately compensates  
340 for disturbances and uncertainties in the process. Moreover, the  $\rho_{min}$  is related  
341 to the minimum joint extension value from the resting position. In this study,  
342 the tests were performed to obtain  $\rho_{max}$  and  $\rho_{min}$  corresponding to  $\theta_{max} = 40^\circ$   
343 and  $\theta_{min} = 10^\circ$ , respectively. Note that we could adopt other values of lower  
344 limb extension, but we consider that it was a suitable value for gait control  
345 application (Nunes et al. (2019)). Lastly,  $\rho_{min}$  and  $\rho_{max}$  were also useful to  
346 select the initial PW and an upper bound to the control signal, respectively. If  
347  $\rho_{max}$  does not approach the saturation value of the stimulator ( $400\mu s$ ), with the  
348 consent of each individual, we select an adequate upper bound to the control  
349 signal for each stimulation session, aiming to minimize the discomfort level to  
350 volunteers.

351 During the experiments, healthy individuals were instructed to relax, to  
352 not influence the leg motion voluntarily, and allow the stimulation to control  
353 it. During electrical stimulation sessions, the individuals could deactivate the  
354 stimulation pulses using a stop button under any uncomfortable situation (as  
355 shown in Fig. 3).

356 In the following two subsections, the experimental setup is detailed. First,  
357 the case of an individual using the proposed methodology for the first time, i.e.,

358 without any previous data, is considered (Subsection 3.4.1). Next, the case of  
359 individuals who participate in more than one rehabilitation session is considered  
360 (Subsection 3.4.2).

### 361 *3.4.1. First session*

362 In the first session of a new patient, a one-minute stimulation test was con-  
363 ducted. In this stimulation, the experimental system identification procedure  
364 was performed by randomly applying PW values belonging to the set of val-  
365 ues mapped to each individual. The electrical PW random value was constant  
366 for a random time between four and seven seconds. Consequently, a new test  
367 has randomness in the domain of the PW of the electrical stimulation as well  
368 as in the time of each stimulation. In this work, the power of muscle acti-  
369 vation by electrical stimulation in paraplegic individuals was greater. Before  
370 the tests were performed, these individuals were not admitted to a rehabilita-  
371 tion research program involving daily electrically stimulated exercise of their  
372 lower limbs. Consequently, under high stimulation intensity, there was only  
373 partial recruitment of synergistic motor units and there was the co-activation of  
374 antagonists (Doucet et al. (2012)). Unfortunately, this is a disadvantage of con-  
375 ventional single-electrode stimulation, whose increased stimulation intensity will  
376 lead to increased muscle fatigue (Laubacher et al. (2017); Maffiuletti (2010)).  
377 To minimize early fatigue in paraplegic individuals (Gregory et al. (2007)), the  
378 total test time was reduced to 40 s.

379 The motivation to adopt this methodology is to map a tracking situation and  
380 recognize the completely nonlinear and time-varying nature of muscles under  
381 long electrical stimulation time. The PW ( $\mu s$ ) and angular position (rad) data  
382 were automatically recorded with a sampling period of 20 ms, i.e.,  $Ts = 0.02$   
383 (s), resulting in datasets with approximately 3000 samples (60 s) at most.

384 Afterward, the identification data were read and manipulated for feeding  
385 up a shallow MLP with one hidden layer. In the literature, one hidden layer  
386 has been proved to be sufficient to approximate any continuous function on a  
387 compact domain (Hornik et al. (1989); Previdi (2002)). We tuned the number

388 of neurons via a random search procedure (Bergstra & Bengio (2012)), in which  
389 a combination of hyperparameters is randomly selected to find the best solution  
390 for the built model. This process was only done for individual H1, which was the  
391 first volunteer for this study, and it took less than 30 min to find an appropriate  
392 architecture to be used for all other individuals. The number of neurons was  
393 selected as 250; hyperbolic tangent activation was used in each neuron from  
394 the hidden layer, and the output layer was composed of one neuron with linear  
395 activation, which gives the estimated output  $\hat{y}(k)$ .

396 We experimented with several  $m$  and  $n$  values, and the one with the best  
397 time-utility trade-off was  $m = n = 1$ . This resulted in datasets containing  
398 the last input value “Pulse\_Width( $k - 1$ )” and the last output value “Angular  
399 Position ( $k - 1$ )” as features, and the actual output value “Angular\_Position  
400 ( $k$ )” as target. The MLP NN model requires a normal input arranged as  
401 [*samples, features*], where the observations at previous time-steps are inputted  
402 as features to the model. In general, the training time of each NN model in the  
403 first session did not exceed 5 min as the number of samples was small ( $\sim 3,000$   
404 for healthy individuals and  $\sim 2,000$  for SCI ones).

405 Therefore, using the estimated model, we performed an optimization pro-  
406 cedure based on the proposed IGA to find the best gains combination for two  
407 reference trajectories. The first trajectory is a sinusoidal wave ranging from  $10^\circ$   
408 to  $40^\circ$  and the second trajectory is a  $40^\circ$  step wave ( $30^\circ$  for individuals with  
409 SCI); the first and second trajectories simulate isotonic and isometric contrac-  
410 tions, respectively. A smooth range of motion at  $40^\circ$  and a small-time period  
411 (sine wave) was used to avoid premature fatigue by diminishing muscle effort.

412 Considering a real-world application of the proposed methodology and by  
413 assuming a limited time for a rehabilitation session, we used the following as the  
414 initial parameters of the IGA simulations: population size  $N_p = 8$ , mutation  
415 rate  $M_r = 0.5$ , number of generations  $N_g = 6$  (size of RIP), and  $k = 1$  iteration.  
416 The algorithm ran only once providing  $N_g$  combination of RISE controller gains.  
417 Generally, the running time did not exceed 10 min of execution.

418 Notice that the proposed IGA in Arcolezi et al. (2019) has a pre-processing

419 step (step 1 of the algorithm), which tries to bound the gain values when apply-  
420 ing the genetic operators (crossover, mutation) to the required stability condi-  
421 tions presented in Subsection 2.2. However, there is still a possibility that given  
422 an identified model and the optimization procedure that gain values deviate  
423 from the required conditions. Yet, as genetic algorithms are population-based,  
424 one can compare and select the most appropriate combination of gains for a  
425 given individual that satisfies the gain’s condition. Before the real experiment,  
426 previous simulations of both trajectories were made to visually inspect the sys-  
427 tem response.

428 Lastly, using empirical gains and the ones encountered by the IGA, the con-  
429 trolling procedure was implemented for both trajectories. Data were recorded  
430 with a sampling period  $Ts = 0.005$  (s), generally resulting in a dataset with  
431 approximately 12,000 samples (60 s) at most.

432 The programming language used in this research was Matlab<sup>®</sup>, both for de-  
433 veloping the optimization algorithm and for the system identification procedure  
434 via NNs. The simulation system was developed using the Matlab/Simulink<sup>®</sup>  
435 platform, which contains both sine and step trajectories, a saturation block to  
436 bound the control signal from  $0 \mu s$  to  $\rho_{max} \mu s$  for each individual, the RISE  
437 controller block, and the identified NN block for each individual.

#### 438 3.4.2. More than one session

439 For individuals who participated in more sessions, with at least 48 hours  
440 of difference between two consecutive sessions, the one-minute stimulation test  
441 (identification step) was not considered, as it was performed when an individual  
442 participated for the first time. The data from previous rehabilitation sessions  
443 were used to train an NN model in an offline scheme. Before a new session, all  
444 data from an individual were combined to a single dataset and used to better  
445 map the relationship between angular position and electrical stimulation. In this  
446 study, we only used the control data resulting from the control-stimulation ses-  
447 sions with fine-tuned IGA gains, as it would be in real life rather than empirical  
448 gains.

449 Thus, using each trained identified model, we performed an optimization  
450 procedure based on the IGA to find the best gain combination for both sine  
451 and step reference trajectories. As this optimization was performed in an offline  
452 scheme and before the next session, time and computational costs were not too  
453 strict as they were for the first session. Therefore, the initial parameters of IGA  
454 used for simulations were as follows: population size  $N_p = 10$ , mutation rate  
455  $M_r = 0.3$ , number of generations  $N_g = 30$  (size of RIP) and  $k = 1$  iteration.  
456 The algorithm ran only once, and several gain combinations from the set of  
457 solutions were simulated to check the system response and select the best gain  
458 combination for both trajectories. Generally, the total time for both system  
459 identification and RISE gains optimization procedures took about 1 *h* for each  
460 individual/session.

461 For the experimental part, the electrodes were positioned at the motor-point  
462 identified in the first session, and similarly, a few open-loop tests, applying a  
463 step input during four seconds, were performed, to determine a bounded PW  
464 band related to  $\theta_{min} = 10^\circ$  and  $\theta_{max} = 40^\circ$ . Afterward, a small-time interval  
465 for muscle rest was provided.

466 Therefore, knowing the fine-tuned gain parameters for each individual, we  
467 applied the controlling procedure for both references, and then employed an  
468 empirical gain combination for comparing results.

#### 469 **4. Results and Discussion**

470 In this section, we report the results obtained by applying our proposed  
471 methodology in real experiments. During this study, individuals H1-H4 partici-  
472 pated in five sessions, H5 in three sessions, and H6-H7 in two sessions. Individ-  
473 uals with SCI participated in only one session due to displacement difficulties.  
474 For all individuals, the first session took more time and one additional stimu-  
475 lation than the subsequent ones. This was due to the one-minute stimulation  
476 test, and the training/optimization time during the session to find the best gain  
477 combination. Before the start of any control-stimulation test, five combina-

478 tions of empirical gains ( $\alpha_1; \alpha_2; ks; \beta$ ) were chosen as (1; 2; 30; 5), (0.5; 1; 30; 1.5),  
479 (0.8; 1.2; 20.5; 2.5), (5; 2; 15; 3), (4; 7; 25; 8) for sessions one to five, respectively.  
480 As the system responses to any combination of gains were unknown, they were  
481 all chosen at random. Subsections 4.1 and 4.2 present our nonlinear control  
482 and system identification results and analysis, respectively. Lastly, we provide  
483 a general discussion in Subsection 4.3.

#### 484 4.1. Control-based NMES results

485 Figures 4 and 5 illustrate the tracking results on both trajectories and their  
486 delivered PWs (Deliv. PWs) for individuals P1 and P2, respectively. Addition-  
487 ally, Table 2 presents control results for the sine wave, comparing the proposed  
488 methodology with an empirical tuning for all individuals (*Ind.*) in each ses-  
489 sion (*Sess.*). The metrics in this table are the root mean square error (RMSE)  
490 between the desired and actual knee angles considering the whole period of  
491 control-stimulation; and the time of effective control (TEC), which represents  
492 how much time in seconds the lower limb was control-stimulated to track the  
493 reference angle. When the lower limb did not track the reference angle, the  
494 RMSE metric is represented by NC, meaning “not calculated”. More precisely,  
495 the TEC metric is the time between the initial control-stimulation until the leg  
496 stops tracking the reference angle ( $\pm 5^\circ$  error) for 5 s. In the worst-case, if the  
497 leg never tracks the reference angle, NC is assigned.

498 Similarly, Table 3 presents control results for the step wave, comparing the  
499 proposed methodology with an empirical tuning for all individuals in each ses-  
500 sion. The metrics in this table are the RMSE, TEC, and the averaged and  
501 standard deviation (std) values of the knee angular position around the operat-  
502 ing point (AvStd. OP) in degrees. The *AvStd. OP* metric will be regarded as an  
503 indicator to evaluate the oscillatory behavior during regulation around an operat-  
504 ion point ( $40^\circ$  for healthy individuals and  $30^\circ$  for individuals with SCI). For  
505 individuals who participated in more than one session, Tables 2 and 3 present  
506 the averaged (Avg.) and the std values for both RMSE and TEC metrics, which  
507 are calculated considering all sessions of each individual. The symbol (\*) indi-



508 cates there is no std value, as there are more “NC” than real values. Lastly,  
 509 similar to Figs. 4 and 5, Appendix A provides supplementary illustrations for  
 510 the tracking results of individuals H1 (session  $v$ ), H2 (session  $ii$ ), and H4 (ses-  
 511 sion  $v$ ), respectively, as well as the fine-tuned gains ( $\alpha_1$ ;  $\alpha_2$ ;  $k_s$ ;  $\beta$ ) used for each  
 512 RISE-based control-stimulation session, in Table A.5.

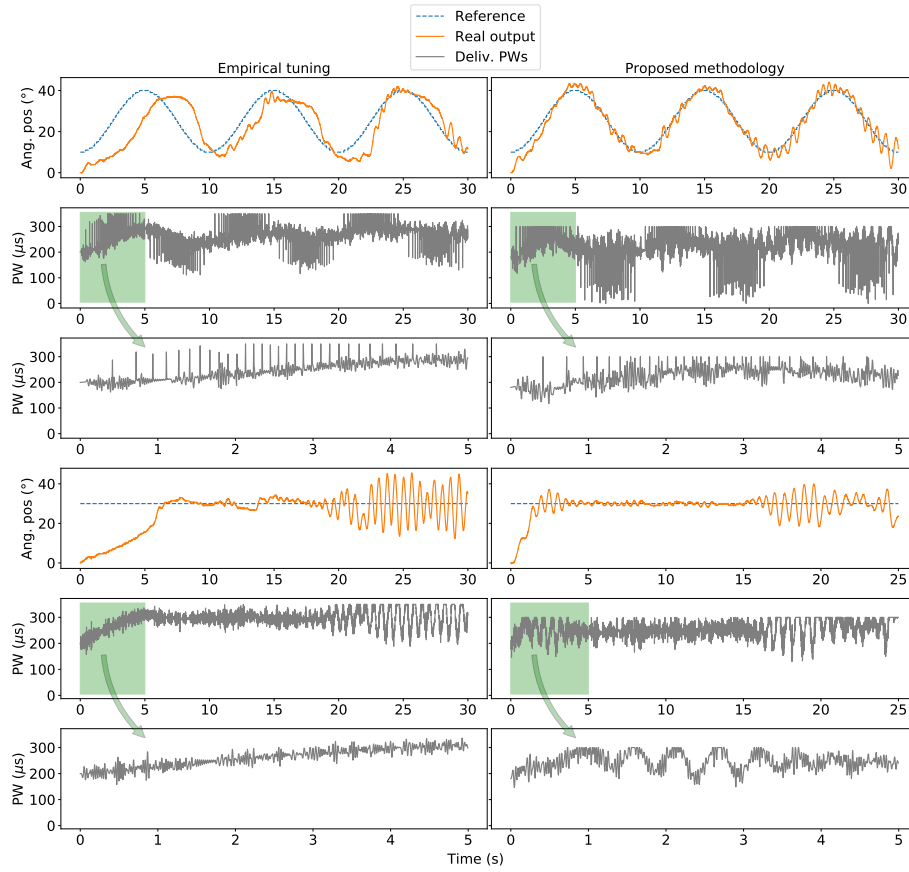


Figure 4: Experimental results for individual P1 comparing empirical gains and the proposed methodology. The first and second rows illustrate the tracking results for the sine wave and the corresponding delivered PWs (with zoom during five seconds on the third row), respectively. Similarly, the fourth and fifth rows illustrate the tracking results for the step wave and the corresponding delivered PWs (with zoom during five seconds on the last row), respectively.

513 As shown in Tables 2 and 3 and Figs. 4 and 5, the proposed methodology  
 514 could be effectively applied to clinical procedures for treating people with SCI

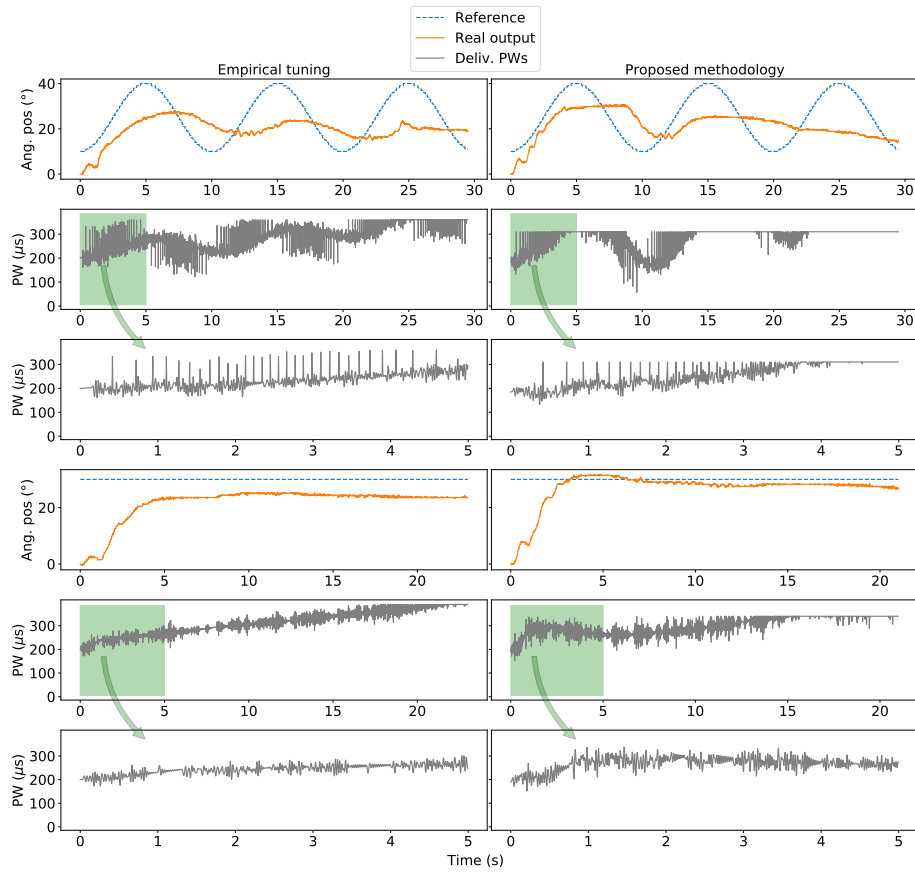


Figure 5: Experimental results for individual P2 comparing empirical gains and the proposed methodology. The first and second rows illustrate the tracking results for the sine wave and the corresponding delivered PWs (with zoom during five seconds on the third row), respectively. Similarly, the fourth and fifth rows illustrate the tracking results for the step wave and the corresponding delivered PWs (with zoom during five seconds on the last row), respectively.

515 via NMES/FES. In general, tremors (mainly for P1) and fatigue were detected  
 516 for both individuals with SCI at the end of each trajectory (sine and wave).  
 517 This was because neither of them had been admitted to a rehabilitation research  
 518 program involving daily electrical stimulation exercise of their lower limbs. In  
 519 all experiments, P1 had no perception of the stimulation, while P2 experienced  
 520 small discomfort due to the electrical stimulation intensity. Results from P1  
 521 validate and substantiate the first hypothesis presenting very good tracking

Table 2: Performance results for the sine wave on control experiments using the proposed methodology and empirical tuning for all individuals in their respective sessions.

Ind.	Sess.	Empirical		Proposed methodology	
		RMSE	TEC	RMSE	TEC
P1	i	9.147°	30 s	2.984°	30 s
P2	i	11.296°	30 s	10.730°	30 s
H1	i	7.494°	60 s	5.830°	60 s
	ii	8.752°	60 s	5.933°	60 s
	iii	14.092°	60 s	7.337°	60 s
	iv	6.377°	60 s	3.629°	60 s
	v	6.383°	60 s	3.562°	60 s
<b>Avg.(std)</b>		8.62(2.87)°	60(0) s	5.26(1.46)°	60(0) s
H2	i	5.212°	60 s	5.055°	45 s
	ii	8.317°	60 s	3.885°	60 s
	iii	11.741°	35 s	3.633°	60 s
	iv	4.887°	40 s	3.562°	40 s
	v	10.713°	33 s	4.858°	23 s
<b>Avg.(std)</b>		8.17(2.78)°	46(12) s	4.20(0.63)°	46(14) s
H3	i	NC	NC	6.019°	30 s
	ii	9.221°	50 s	7.615°	50 s
	iii	NC	NC	4.616°	33 s
	iv	3.775°	33 s	6.688°	60 s
	v	19.096°	60 s	6.516°	60 s
<b>Avg.(std)</b>		10.70(6.3)°	48(11) s	6.29(0.98)°	47(13)s
H4	i	NC	NC	9.382°	60 s
	ii	12.794°	60 s	4.823°	60 s
	iii	8.246°	60 s	4.640°	30 s
	iv	3.534°	31 s	4.561°	60 s
	v	16.483°	60 s	3.717°	42 s
<b>Avg.(std)</b>		10.3(4.86)°	53(13) s	5.42(2.01)°	50(12) s
H5	i	NC	NC	6.006°	20 s
	ii	8.070°	50 s	3.017°	21 s
	iii	NC	NC	3.872°	52 s
<b>Avg.(std)</b>		8.070(*)°	50(*) s	4.30(1.26)°	31(15)s
H6	i	NC	NC	10.128°	60 s
	ii	9.105°	60 s	6.553°	60 s
<b>Avg.(std)</b>		9.105(*)°	60(*) s	8.34(1.79)°	60(0)s
H7	i	NC	NC	8.500°	60 s
	ii	NC	NC	6.630°	50 s
<b>Avg.(std)</b>		NC	NC	7.56(0.94)°	55(5) s

522 results using the proposed methodology. When empirical gains were used, the  
523 lower limb tracked the sine wave with a lag and presented a slow response to

Table 3: Performance results for the step wave on control experiments using the proposed methodology and empirical tuning for all individuals in their respective sessions.

Ind.	Sess.	Empirical			Proposed methodology		
		RMSE	TEC	AvStd. OP	RMSE	TEC	AvStd. OP
P1	i	10.995°	30 s	29.44(6.03)°	5.978°	25 s	29.88(3.25)°
P2	i	10.106°	23 s	24.15(0.59)°	6.613°	21 s	28.51(0.99)°
H1	i	5.920°	60 s	39.35(2.50)°	6.167°	60 s	39.54(1.63)°
	ii	12.291°	60 s	36.19(6.92)°	8.201°	60 s	39.54(4.61)°
	iii	7.266°	60 s	37.61(3.76)°	4.164°	60 s	39.98(1.48)°
	iv	6.741°	60 s	38.70(4.59)°	4.404°	60 s	39.89(1.64)°
	v	6.887°	60 s	39.94(5.88)°	4.425°	60 s	40.01(1.34)°
<b>Avg.(std)</b>		7.82(2.28)°	60(0) s	-	5.47(1.54)°	60(0) s	-
H2	i	9.764°	35 s	38.45(2.00)°	6.212°	37 s	39.80(2.50)°
	ii	NC	NC	NC	7.856°	25 s	38.05(1.53)°
	iii	11.822°	57 s	33.50(4.14)°	5.457°	37 s	39.88(3.36)°
	iv	6.424°	34 s	38.94(1.92)°	4.890°	45 s	39.42(1.33)°
	v	6.226°	35 s	39.83(4.11)°	7.233°	38 s	40.19(3.34)°
<b>Avg.(std)</b>		8.56(2.35)°	46(11) s	-	6.33(1.09)°	37(6) s	-
H3	i	15.359°	48 s	32.47(7.59)°	8.176°	32 s	39.54(1.34)°
	ii	8.230°	45 s	38.53(2.19)°	5.598°	28 s	39.71(0.63)°
	iii	14.233°	38 s	33.06(6.26)°	6.258°	30 s	39.66(0.95)°
	iv	5.472°	40 s	39.54(0.71)°	6.357°	55 s	39.64(5.21)°
	v	7.102°	60 s	39.88(6.52)°	4.491°	60 s	39.84(2.23)°
<b>Avg.(std)</b>		10.08(3.97)°	46(8) s	-	6.18(1.2)°	41(14) s	-
H4	i	13.914°	60 s	39.08(9.81)°	5.943°	60 s	40.02(2.97)°
	ii	8.354°	60 s	40.49(2.82)°	4.694°	60 s	40.00(0.87)°
	iii	8.830°	60 s	42.26(1.86)°	7.286°	60 s	39.92(2.35)°
	iv	4.551°	60 s	39.89(1.47)°	6.777°	60 s	39.82(5.33)°
	v	7.871°	60 s	39.92(7.29)°	4.895°	60 s	39.88(2.52)°
<b>Avg.(std)</b>		8.70(3.01)°	60(0) s	-	5.92(1.02)°	60(0) s	-
H5	i	NC	NC	NC	5.719°	60 s	39.83(3.74)°
	ii	8.076°	52 s	39.13(2.43)°	5.481°	50 s	39.58(1.11)°
	iii	13.032°	45 s	33.66(5.39)°	6.351°	50 s	39.42(1.99)°
<b>Avg.(std)</b>		10.55(2.48)°	47(3) s	-	5.85(0.37)°	57(5) s	-
H6	i	12.789°	60 s	31.64(5.37)°	6.578°	60 s	40.01(2.80)°
	ii	7.506°	60 s	39.6(2.89)°	4.040°	60 s	39.62(1.49)°
<b>Avg.(std)</b>		10.15(2.64)°	60(0) s	-	5.31(1.27)°	60(0) s	-
H7	i	9.554°	40 s	38.82(4.25)°	7.044°	21 s	39.63(2.49)°
	ii	13.135°	60 s	36.38(10.51)°	5.212°	60 s	40.04(1.68)°
<b>Avg.(std)</b>		11.34(1.79)°	50(10) s	-	6.13(0.92)°	40(19) s	-

524 the step trajectory. Moreover, the RMSE of 2.9842° for the IGA sine wave  
525 from P1 was the best result during all experiments in this research, which is

526 a third of the RMSE obtained using empirical gains  $9.1471^\circ$ . However, in the  
527 final seconds (about 28 s), the lower limb would start to have more tremors due  
528 to the fatigue factor; this is also noticed after about 15 s to the step wave for  
529 both our proposed method and empirical tuning.

530 Furthermore, the tracking result for the sine wave of individual P2 was not as  
531 satisfactory such as for P1. However, as seen in the Deliv. PWs curve (Fig. 5),  
532 this poor sine wave tracking could be due to an underestimation for the upper  
533 bound to the control signal value (as this individual experienced discomfort  
534 under NMES); selecting a higher value may have resulted in good tracking.  
535 This inference is substantiated by the good results achieved in the step wave  
536 after a 3 min interval for muscle rest and by having consent to increase the  
537 upper bound value to the PW. A good regulation around the operation point  
538 was achieved for approximately 21 s, with 50% less RMSE than that obtained  
539 using empirical tuning. More specifically, using empirical tuning led to poor  
540 performances for both sine and step trajectories, as the leg did not track the  
541 sine wave, and the regulation around the operation point featured a stationary  
542 error.

543 For healthy individuals, as seen in Tables 2 and 3 and in the figures of Ap-  
544 pendix A, using empirical gains led to several poor performances. In many tests,  
545 the control-stimulated lower limb did not track the reference angle (“NC”) or  
546 presented high oscillatory compartment. This problem is, for example, demon-  
547 strated in Figs. A.10 and A.12 and in Table 3 regarding the *AvStd. OP* metric,  
548 as using empirical gains resulted in average values (knee angular position) below  
549 the operation point with high std values. When the proposed methodology was  
550 used, for all individuals, satisfactory and suitable tracking results were acquired  
551 for both the tracking of sine wave via isotonic contraction and the regulation  
552 around an operation point (step wave) as isometric contraction. On average, for  
553 each individual, our proposed methodology presented much lower RMSE while  
554 still achieving high TEC (Tables 2 and 3).

555 Finally, for most healthy individuals, when our proposed solution was used  
556 and RISE controller was not tuned with empirical gains, the lower limb robustly

557 tried to track the reference angle for 60 s. This could not be possible if we  
558 had performed pretrial tests, which could generate muscle fatigue due to prior  
559 stimulations. In contrast, RISE controller presented by Stegath et al. (2007) and  
560 Stegath et al. (2008) demonstrated tracking control for 8 s for a step trajectory  
561 and 20 s for a sine wave; Sharma et al. (2009) and Sharma et al. (2012) presented  
562 tracking control for 30 s for a step- and a sine-type signal; Kushima et al.  
563 (2015) presented tracking control for 30 s for a sine wave, and Downey et al.  
564 (2015) presented tracking control for 45 s (for conventional stimulation) for a  
565 sine trajectory. On the other hand, in some of our experiments, significant  
566 “chattering” was noticed in the control input. Yet, except for individual P2,  
567 none of the other voluntary participants reported discomfort due to NMES  
568 while presenting satisfactory tracking of the lower limb with high TEC. Further  
569 improvements to RISE controller tuning (i.e., IGA) may help to smooth this  
570 “chattering” problem, which is undesirable and may lead to poor controller  
571 performance (Lynch & Popovic (2012)).

#### 572 4.2. Nonlinear system identification results

573 Table 4 presents the following metrics for all individuals (*Ind.*) in each ses-  
574 sion (*Sess.*): (i) the Pearson correlation coefficient (*Corr.*) between the input  
575 (PW) and output (angular position) data using past control data as sessions  
576 progress; (ii) the Coefficient of determination ( $R^2$ ); and (iii) the mean squared  
577 error (*MSE*). These metrics are explained in the following: First, the *Corr.* be-  
578 tween the input and output data indicates the correlation between both data,  
579 which clarifies how “difficult” it is to identify the system dynamics. More specif-  
580 ically, *Corr.* measures the linear correlation between two variables  $x$  and  $y$ . The  
581 *Corr.* value ranges from -1 to 1. The higher the value, the stronger the corre-  
582 lation. A negative value indicates an inverse correlation, while a positive value  
583 indicates a regular correlation. Second, the coefficient of determination ( $R^2$ ) is  
584 the proportion of the variance in the dependent variable that is predictable from  
585 the independent variable. The larger  $R^2$  is, the more the variability is indicated

586 by the linear regression model<sup>1</sup>. Third, the MSE is the average squared error  
 587 between the NN outputs and the real ones.

588 Additionally, Figs. 6 and 7 compare the results from simulation and real  
 589 experiments using either empirical or fine-tuned IGA gains. These figures were  
 590 selected for illustration purposes only, as the objective is to highlight the benefits  
 591 of using past data for the nonlinear system identification step. In Appendix A,  
 592 we provide more illustrations comparing simulation versus the real experiment  
 593 results.

Table 4: Identification results for all individuals in their respective sessions.

Ind.	Sess.	Corr.	$R^2$	MSE	Ind.	Sess.	Corr.	$R^2$	MSE
P1	i	0.4153	0.836	0.001	P2	i	0.1035	0.796	0.003
	i	0.5908	0.726	0.002		i	0.7789	0.869	0.006
	ii	0.1738	0.157	0.038		ii	0.2594	0.416	0.039
H1	iii	0.0469	0.101	0.042	H2	iii	0.2640	0.308	0.039
	iv	-0.1109	0.159	0.041		iv	0.2606	0.282	0.037
	v	-0.0916	0.113	0.040		v	0.2769	0.292	0.038
	i	0.8333	0.820	0.003		i	0.7339	0.974	0.001
	ii	0.4325	0.498	0.023		ii	0.0476	0.377	0.054
H3	iii	0.3083	0.506	0.023	H4	iii	-0.1050	0.323	0.054
	iv	0.3523	0.510	0.024		iv	-0.0502	0.294	0.052
	v	0.2650	0.492	0.026		v	-0.1017	0.281	0.049
	i	0.6738	0.881	0.001		i	0.7182	0.815	0.001
H5	ii	0.3774	0.682	0.030	H6	ii	0.3078	0.476	0.028
	iii	0.3458	0.599	0.035		-	-	-	-
	i	0.5201	0.767	0.004		-	-	-	-
H7	ii	0.5520	0.476	0.017		-	-	-	-

594 As presented in Table 4, there are considerable decrements in the *Corr.*  
 595 between the input and output data as sessions progress (given the addition of  
 596 control data from every new session). Moreover, while the data from healthy  
 597 individuals in the first session are highly correlated ( $0.5201 \leq Corr. \leq 0.8333$ ),  
 598 the ones from individuals with SCI are poorly correlated, as their muscles do  
 599 not respond to NMES/FES as well as the muscles of the healthy individuals.  
 600 Moreover, due to less correlation between data, the generalization and learning

<sup>1</sup><https://fr.mathworks.com/help/stats/coefficient-of-determination-r-squared.html>

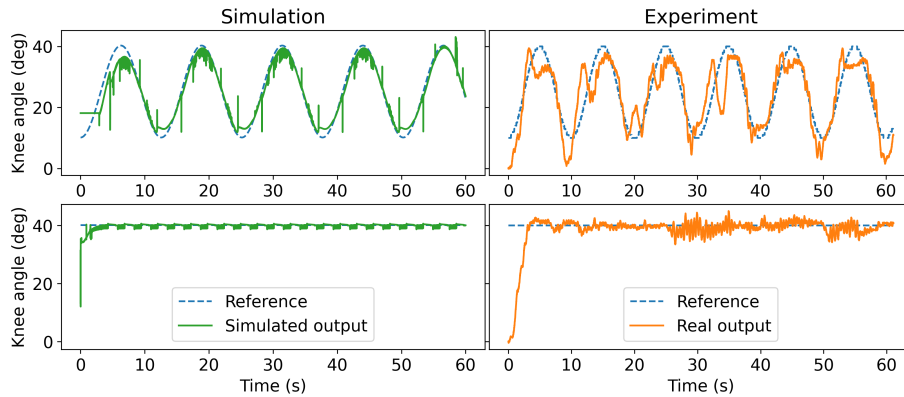


Figure 6: Comparison of simulation and real experiments for individual H1 using past rehabilitation data to identify the nonlinear model.

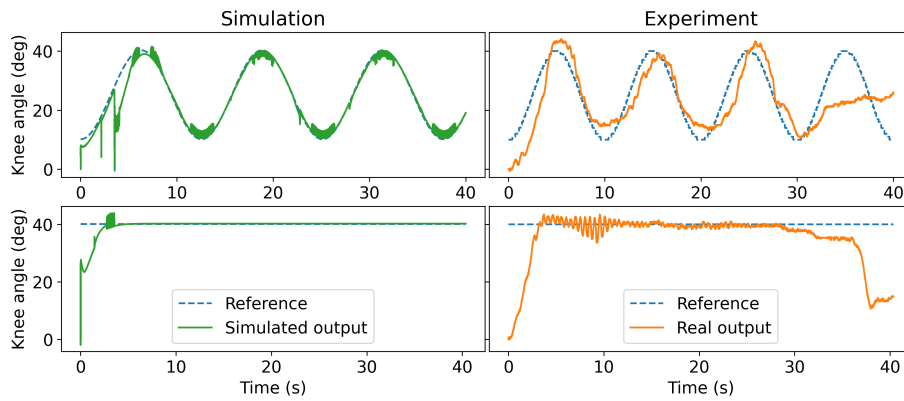


Figure 7: Comparison of simulation and real experiments for individual H3 using past rehabilitation data to identify the nonlinear model.

601 procedure of an NN is harder, which resulted in increments in the error metrics  
 602  $R^2$  and  $MSE$ . However, as shown in the Figs. 6 and 7, these models better  
 603 describe what happens in real experiments, where non-ideal conditions such as  
 604 fatigue, tremors, and spasms, are explained by data.

605 As shown in Figs. 6 and 7, the identified models simulated a sine trajectory  
 606 with some tremors in the upper and lower peak values and some tremors to  
 607 the step wave around the operation point. These behaviors were also noticed  
 608 in real experiments. Appendix A presents simulations to the step wave with



609 a quick response and with oscillatory behavior for the whole period, which was  
610 also verified in real experiments. Although not flawless, such models can provide  
611 more insights into the real system response. However, as approximate models of  
612 healthy individuals, neither of them would be suitable for an exact description of  
613 the real system; for instance, voluntary movements, fear, or other issues related  
614 to the individual thoughts (e.g., social or personal life), can affect results, and  
615 these aspects could not be predicted by the model.

#### 616 *4.3. Discussion*

617 Because this research was conducted with volunteering participants, we de-  
618 pended on their availability. For instance, not all healthy individuals partic-  
619 ipated in the pre-established five sessions. One volunteer showed availability  
620 to participate in only two sessions (H7), two volunteers showed availability to  
621 participate in only three sessions (H5 and H6), while the others (H1-H4) par-  
622 ticipated in all five sessions. This way, rather than excluding the non-uniform  
623 collected data, we preferred to present our results for all volunteers according to  
624 the number of sessions they participated in. Note that this procedure is common  
625 in studies in this area, because each session depends on consent, as established  
626 by the ethics committee.

627 Figures 8 and 9 summarize the results of Tables 2 and 3 by illustrating in  
628 bar plots the RMSE metric for both the empirical tuning and our proposed  
629 methodology, considering each trajectory (sine and step) in all sessions and all  
630 individuals. In these figures, “NC” indicates when the leg did not track the  
631 reference angle. Omitted bars indicate the individual did not participate in the  
632 corresponding session.

633 As demonstrated in Figs. 8 and 9, the proposed methodology consistently  
634 and considerably outperforms the empirical tuning approach, which supports  
635 and validates the first hypothesis made in this paper. Additionally, in the  
636 first sessions of healthy individuals, the RMSEs were generally higher, which  
637 could be due to fear or discomfort to the electrical stimulation or voluntary  
638 movements. However, as sessions progressed, the tracking results improved for

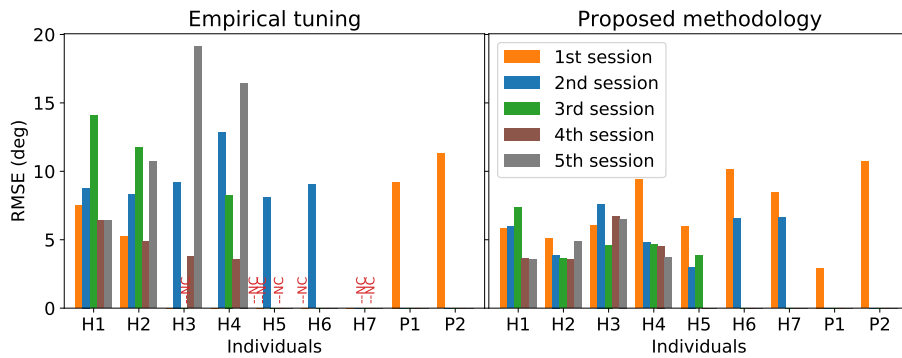


Figure 8: RMSE analysis for the sine trajectory based on empirical tuning or the proposed methodology.

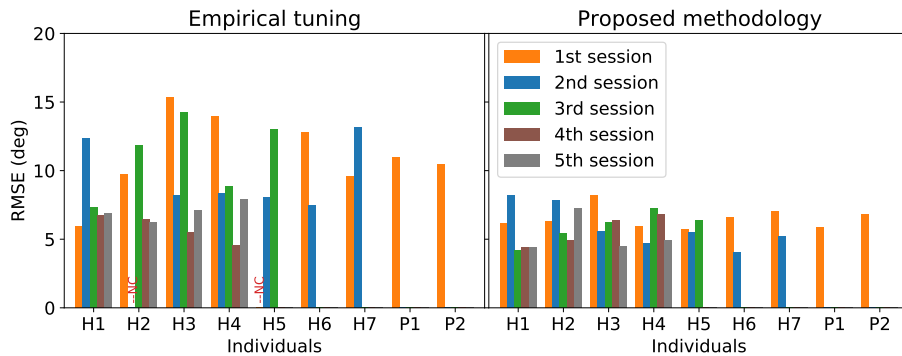


Figure 9: RMSE analysis for the step trajectory based on empirical tuning or the proposed methodology.

639 some individuals, which among many factors, can be explained by the use of  
 640 a more representative model with past rehabilitation data. This resulted in a  
 641 better tuning of the RISE controller improving the tracking results in practice.

642 More precisely, considering the first hypothesis made in this paper, setting  
 643 empirical gains to RISE controller generally led to an underperformance compared  
 644 with the use of ML-based algorithms to find the best combination for  
 645 each individual. That is, to provide efficient treatment for individuals with SCI  
 646 via NMES/FES, a fine-tuning method such as the presented methodology can  
 647 prevent SCI patients from experiencing premature fatigue and other problems

648 during rehabilitation.

649 Moreover, for the second hypothesis, the use of the past rehabilitation data  
650 for the nonlinear system identification task also presented promising results.  
651 Even though there is less correlation between the input and output data, which  
652 increases the error on the identification process, the identified models “gained”  
653 implicit non-ideal conditions such as tremors and spasms (*cf.*, Figs. 6 and 7  
654 and figures in Appendix A). Therefore, using data from past rehabilitation  
655 sessions of each individual and strong tools, such as NNs, the mapping over  
656 the delivered electrical stimulation and the angular position can be efficiently  
657 addressed with more realistic models. Regarding future work, we recommend  
658 and intend to explore a deeper comparison between a case considering past  
659 rehabilitation data and a case considering each session of an individual as the  
660 first one (applying and using only the one-minute stimulation test for system  
661 identification).

662 Finally, in the NMES-based knee simulation system, using data saved from  
663 each patient allows testing improvements to RISE control law and testing more  
664 control techniques before actual implementation, saving time and resources.  
665 Furthermore, the proposed methodology for knee joint control would allow peo-  
666 ple with no experience with technical information on neural networks, genetic  
667 algorithms, or even the control law RISE to easily use a closed-loop NMES/FES  
668 system for SCI individuals’ rehabilitation.

## 669 5. Conclusion

670 Aiming to improve human lower limb tracking control of individuals with  
671 SCI via NMES/FES, this paper introduces a novel ML-based methodology. It  
672 consists of data-driven models that use past rehabilitation data, the RISE con-  
673 trol method (or fundamentally similar control laws) to guarantee the semi-global  
674 asymptotic stability, and an improved genetic algorithm to efficiently tune the  
675 controller. Experiments were performed with seven healthy and two paraplegic  
676 individuals, which validated the proposed methodology.

677 Additionally, RISE control method designed for lower limb control in the  
678 literature did not validate this RISE controller for paraplegic subjects. There-  
679 fore, for the first time and using the proposed methodology, we validated this  
680 controller with two SCI subjects with promising tracking results. This, however,  
681 would not be possible using a “trial and error” method by fatiguing the muscle  
682 before acquiring good tuning. Moreover, in the experiments performed in this  
683 research, for many healthy individuals, the lower limb robustly tried to track  
684 the reference angle for more than 45 s, which is the maximum time presented  
685 in the literature for RISE controller, reaching 60 s many times.

686 We recommend and intend to explore the following areas for future work:  
687 a deeper validation with SCI patients under more sessions; a comparison of  
688 the effectiveness of using past rehabilitation data with different setups, e.g.,  
689 the SCI patient is identified each session; the implementation of deeper and  
690 dynamic NNs studied in Arcolezi et al. (2020) to improve identified models in our  
691 proposed methodology; to improve the RISE controller tuning approach (i.e.,  
692 IGA algorithm); the consideration of different control laws and improvements  
693 to RISE control method.

#### 694 **Acknowledgment**

695 This work was supported by the Coordenação de Aperfeiçoamento de Pessoal de  
696 Nível Superior - Brasil (CAPES) - Finance Code 001, by the Brazilian National  
697 Council for Scientific and Technological Development (CNPq) under research  
698 fellowships 309.872/2018-9 and 312.170/2018-1, and by the Region of Bourgogne  
699 Franche-Comté CADRAN Project. The authors would also like to thank each  
700 volunteer who participated in this research, especially those with spinal cord  
701 injury. We also thank anonymous reviewers for several comments that led to  
702 improvements in the paper as well as Enago for the English language review.

703 **References**

- 704 Arcolezi, H. H., Nunes, W. R. B. M., Cerna, S., de Araujo, R. A., Sanches, M.  
705 A. A., Teixeira, M. C. M., & de Carvalho, A. A. (2020). Identifying the knee  
706 joint angular position under neuromuscular electrical stimulation via long  
707 short-term memory neural networks. *Research on Biomedical Engineering*, .  
708 doi:10.1007/s42600-020-00089-1.
- 709 Arcolezi, H. H., Nunes, W. R. B. M., Nahuis, S. L. C., Sanches, M. A. A.,  
710 Teixeira, M. C. M., & de Carvalho, A. A. (2019). A RISE-based controller  
711 fine-tuned by an improved genetic algorithm for human lower limb rehabilita-  
712 tion via neuromuscular electrical stimulation. In *2019 6th International Con-*  
713 *ference on Control, Decision and Information Technologies (CoDIT)*. IEEE.  
714 doi:10.1109/codit.2019.8820357.
- 715 Bergstra, J., & Bengio, Y. (2012). Random search for hyper-parameter opti-  
716 mization. *JMLR*, (p. 305).
- 717 Bickenbach, J. (2013). *International perspectives on spinal cord injury*. Geneva,  
718 Switzerland: World Health Organization.
- 719 Chen, S., Billings, S. A., & Grant, P. M. (1990). Non-linear system identifica-  
720 tion using neural networks. *International Journal of Control*, *51*, 1191–1214.  
721 doi:10.1080/00207179008934126.
- 722 Cheng, T.-H., Wang, Q., Kamalapurkar, R., Dinh, H. T., Bellman, M., &  
723 Dixon, W. E. (2016). Identification-based closed-loop NMES limb tracking  
724 with amplitude-modulated control input. *IEEE Transactions on Cybernetics*,  
725 *46*, 1679–1690. doi:10.1109/tycb.2015.2453402.
- 726 Chu, S., Shoureshi, R., & Tenorio, M. (1990). Neural networks for system  
727 identification. *IEEE Control Systems Magazine*, *10*, 31–35. doi:10.1109/37.  
728 55121.

- 729 Doucet, B., Lam, A., & Griffin, L. (2012). Neuromuscular electrical stimulation  
730 for skeletal muscle function. *The Yale journal of biology and medicine*, *85*,  
731 201–215.
- 732 Downey, R. J., Cheng, T.-H., Bellman, M. J., & Dixon, W. E. (2015). Closed-  
733 loop asynchronous neuromuscular electrical stimulation prolongs functional  
734 movements in the lower body. *IEEE Transactions on Neural Systems and Re-*  
735 *habilitation Engineering*, *23*, 1117–1127. doi:10.1109/tnsre.2015.2427658.
- 736 Downey, R. J., Cheng, T.-H., & Dixon, W. E. (2013). Tracking control of a  
737 human limb during asynchronous neuromuscular electrical stimulation. In  
738 *52nd IEEE Conference on Decision and Control*. IEEE. doi:10.1109/cdc.  
739 2013.6759872.
- 740 Ferrarin, M., Palazzo, F., Riener, R., & Quintern, J. (2001). Model-based control  
741 of FES-induced single joint movements. *IEEE Transactions on Neural Sys-*  
742 *tems and Rehabilitation Engineering*, *9*, 245–257. doi:10.1109/7333.948452.
- 743 Gaino, R., Covacic, M., Teixeira, M., Cardim, R., Assunção, E., de Carvalho, A.,  
744 & Sanches, M. (2017). Electrical stimulation tracking control for paraplegic  
745 patients using t-s fuzzy models. *Fuzzy Sets and Systems*, *314*, 1–23. doi:10.  
746 1016/j.fss.2016.06.005.
- 747 Gaino, R., Covacic, M. R., Cardim, R., Sanches, M. A. A., Carvalho, A. A. D.,  
748 Biazeto, A. R., & Teixeira, M. C. M. (2020). Discrete takagi-sugeno fuzzy  
749 models applied to control the knee joint movement of paraplegic patients.  
750 *IEEE Access*, *8*, 32714–32726. doi:10.1109/access.2020.2971908.
- 751 Gobbo, M., Maffiuletti, N. A., Orizio, C., & Minetto, M. A. (2014). Muscle  
752 motor point identification is essential for optimizing neuromuscular electrical  
753 stimulation use. *Journal of NeuroEngineering and Rehabilitation*, *11*, 17.  
754 doi:10.1186/1743-0003-11-17.
- 755 Gregory, C. M., Dixon, W., & Bickel, C. S. (2007). Impact of varying pulse

- 756 frequency and duration on muscle torque production and fatigue. *Muscle &*  
757 *Nerve*, 35, 504–509. doi:10.1002/mus.20710.
- 758 Hmed, A. B., Bakir, T., Garnier, Y., Binczak, S., & Sakly, A. (2017). A novel  
759 strategy for adjusting current pulse amplitude of FES-systems with PID based  
760 on PSO algorithm method to control the muscle force. In *Proceedings of the*  
761 *14th International Conference on Informatics in Control, Automation and*  
762 *Robotics*. SCITEPRESS - Science and Technology Publications. doi:10.  
763 5220/0006473306640669.
- 764 Ho, C. H., Triolo, R. J., Elias, A. L., Kilgore, K. L., DiMarco, A. F., Bogie,  
765 K., Vette, A. H., Audu, M. L., Kobetic, R., Chang, S. R., Chan, K. M.,  
766 Dukelow, S., Bourbeau, D. J., Brose, S. W., Gustafson, K. J., Kiss, Z. H., &  
767 Mushahwar, V. K. (2014). Functional electrical stimulation and spinal cord  
768 injury. *Physical Medicine and Rehabilitation Clinics of North America*, 25,  
769 631–654. doi:10.1016/j.pmr.2014.05.001.
- 770 Hornik, K., Stinchcombe, M., & White, H. (1989). Multilayer feedforward net-  
771 works are universal approximators. *Neural Networks*, 2, 359–366.
- 772 Jezernik, S., Wassink, R., & Keller, T. (2004). Sliding mode closed-loop control  
773 of FES: Controlling the shank movement. *IEEE Transactions on Biomedical*  
774 *Engineering*, 51, 263–272. doi:10.1109/tbme.2003.820393.
- 775 Kapadia, N., Moineau, B., & Popovic, M. R. (2020). Functional electrical stim-  
776 ulation therapy for retraining reaching and grasping after spinal cord injury  
777 and stroke. *Frontiers in Neuroscience*, 14, 718.
- 778 Kawai, Y., Downey, R. J., Kawai, H., & Dixon, W. E. (2014). Co-contraction  
779 of antagonist bi-articular muscles for tracking control of human limb. In *2014*  
780 *American Control Conference*. IEEE. doi:10.1109/acc.2014.6859102.
- 781 Khadra, F. A., Qudeiri, J. A., & Alkahtani, M. (2016). Optimization of the  
782 parameters of RISE feedback controller using genetic algorithm. *Mathematical*  
783 *Problems in Engineering*, 2016, 1–9. doi:10.1155/2016/3863147.

- 784 Kushima, Y., Kawataka, K., Kawai, H., Kawai, Y., & Dixon, W. E. (2015).  
785 FES knee bending and stretching system with RISE-based tracking control  
786 for human limb. In *2015 IEEE Conference on Control Applications (CCA)*.  
787 IEEE. doi:10.1109/cca.2015.7320727.
- 788 Laubacher, M., Aksöz, A. E., Riener, R., Binder-Macleod, S., & Hunt, K. J.  
789 (2017). Power output and fatigue properties using spatially distributed se-  
790 quential stimulation in a dynamic knee extension task. *European Journal of*  
791 *Applied Physiology*, *117*, 1787–1798. doi:10.1007/s00421-017-3675-0.
- 792 Lew, B., Alavi, N., Randhawa, B. K., & Menon, C. (2016). An exploratory in-  
793 vestigation on the use of closed-loop electrical stimulation to assist individuals  
794 with stroke to perform fine movements with their hemiparetic arm. *Frontiers*  
795 *in Bioengineering and Biotechnology*, *4*. doi:10.3389/fbioe.2016.00020.
- 796 Lynch, C. L., & Popovic, M. R. (2008). Functional electrical stimulation. *IEEE*  
797 *Control Systems*, *28*, 40–50. doi:10.1109/mcs.2007.914689.
- 798 Lynch, C. L., & Popovic, M. R. (2012). A comparison of closed-loop control al-  
799 gorithms for regulating electrically stimulated knee movements in individuals  
800 with spinal cord injury. *IEEE Transactions on Neural Systems and Rehabili-*  
801 *tation Engineering*, *20*, 539–548. doi:10.1109/tnsre.2012.2185065.
- 802 Maffiuletti, N. A. (2010). Physiological and methodological considerations for  
803 the use of neuromuscular electrical stimulation. *European Journal of Applied*  
804 *Physiology*, *110*, 223–234. doi:10.1007/s00421-010-1502-y.
- 805 Makkar, C., Hu, G., Sawyer, W. G., & Dixon, W. E. (2007). Lyapunov-  
806 based tracking control in the presence of uncertain nonlinear parameteri-  
807 zable friction. *IEEE Transactions on Automatic Control*, *52*, 1988–1994.  
808 doi:10.1109/TAC.2007.904254.
- 809 Marquez-Chin, C., & Popovic, M. R. (2020). Functional electrical stimulation  
810 therapy for restoration of motor function after spinal cord injury and stroke:  
811 a review. *BioMedical Engineering OnLine*, *19*, 1–25.



- 812 Mohammed, S., Poignet, P., Fraisse, P., & Guiraud, D. (2012). Toward lower  
813 limbs movement restoration with input-output feedback linearization and  
814 model predictive control through functional electrical stimulation. *Control Engineering Practice*, *20*, 182–195. doi:10.1016/j.conengprac.2011.  
815 10.010.  
816
- 817 Müller, P., Balligand, C., Seel, T., & Schauer, T. (2017). Iterative learning  
818 control and system identification of the antagonistic knee muscle complex  
819 during gait using functional electrical stimulation. *IFAC-PapersOnLine*, *50*,  
820 8786–8791. doi:10.1016/j.ifacol.2017.08.1738.
- 821 Narendra, K., & Parthasarathy, K. (1990). Identification and control of dynam-  
822 ical systems using neural networks. *IEEE Transactions on Neural Networks*,  
823 *1*, 4–27. doi:10.1109/72.80202.
- 824 Nunes, W. R. B. M., Teodoro, R. G., Sanches, M. A. A., de Araujo, R. A.,  
825 Teixeira, M. C. M., & Carvalho, A. A. (2019). Switched controller applied  
826 to functional electrical stimulation of lower limbs under fatigue conditions: A  
827 linear analysis. In *XXVI Brazilian Congress on Biomedical Engineering* (pp.  
828 383–390). Springer Singapore. doi:10.1007/978-981-13-2119-1\_59.
- 829 Page, A., & Freeman, C. (2020). Point-to-point repetitive control of functional  
830 electrical stimulation for drop-foot. *Control Engineering Practice*, *96*, 104280.  
831 doi:10.1016/j.conengprac.2019.104280.
- 832 Patre, P. M., MacKunis, W., Makkar, C., & Dixon, W. E. (2008). Asymp-  
833 totic tracking for systems with structured and unstructured uncertainties.  
834 *IEEE Transactions on Control Systems Technology*, *16*, 373–379. doi:10.  
835 1109/TCST.2007.908227.
- 836 Peckham, P. H., & Knutson, J. S. (2005). Functional electrical stimulation for  
837 neuromuscular applications. *Annual Review of Biomedical Engineering*, *7*,  
838 327–360. doi:10.1146/annurev.bioeng.6.040803.140103.

- 839 Popović, D. B. (2014). Advances in functional electrical stimulation (FES).  
840 *Journal of Electromyography and Kinesiology*, *24*, 795–802. doi:10.1016/j.  
841 jelek.2014.09.008.
- 842 Previdi, F. (2002). Identification of black-box nonlinear models for lower limb  
843 movement control using functional electrical stimulation. *Control Engineering*  
844 *Practice*, *10*, 91–99. doi:10.1016/s0967-0661(01)00128-9.
- 845 Previdi, F., & Carpanzano, E. (2003). Design of a gain scheduling con-  
846 troller for knee-joint angle control by using functional electrical stimula-  
847 tion. *IEEE Transactions on Control Systems Technology*, *11*, 310–324.  
848 doi:10.1109/tcst.2003.810380.
- 849 dos Santos, N. M., Gaino, R., Covacic, M. R., Teixeira, M. C. M., de Car-  
850 valho, A. A., Assunção, E., Cardim, R., & Sanches, M. A. A. (2015). Ro-  
851 bust control of the knee joint angle of paraplegic patients considering norm-  
852 bounded uncertainties. *Mathematical Problems in Engineering*, *2015*, 1–8.  
853 doi:10.1155/2015/736246.
- 854 Sharma, N., Gregory, C. M., Johnson, M., & Dixon, W. E. (2012). Closed-loop  
855 neural network-based NMES control for human limb tracking. *IEEE Transac-*  
856 *tions on Control Systems Technology*, *20*, 712–725. doi:10.1109/tcst.2011.  
857 2125792.
- 858 Sharma, N., Stegath, K., Gregory, C., & Dixon, W. (2009). Nonlinear neu-  
859 romuscular electrical stimulation tracking control of a human limb. *IEEE*  
860 *Transactions on Neural Systems and Rehabilitation Engineering*, *17*, 576–  
861 584. doi:10.1109/tnsre.2009.2023294.
- 862 Stegath, K., Sharma, N., Gregory, C. M., & Dixon, W. E. (2007). Experimental  
863 demonstration of RISE-based NMES of human quadriceps muscle. In *2007*  
864 *IEEE/NIH Life Science Systems and Applications Workshop*. IEEE. doi:10.  
865 1109/lssa.2007.4400880.

- 866 Stegath, K., Sharma, N., Gregory, C. M., & Dixon, W. E. (2008). Nonlinear  
867 tracking control of a human limb via neuromuscular electrical stimulation. In  
868 *2008 American Control Conference*. IEEE. doi:10.1109/acc.2008.4586776.
- 869 Teodoro, R. G., Nunes, W. R., de Araujo, R. A., Sanches, M. A., Teixeira, M. C.,  
870 & de Carvalho, A. A. (2020). Robust switched control design for electrically  
871 stimulated lower limbs: A linear model analysis in healthy and spinal cord  
872 injured subjects. *Control Engineering Practice*, *102*, 104530. doi:10.1016/j.  
873 conengprac.2020.104530.
- 874 Utkin, V. I. (2013). *Sliding modes in control and optimization*. Springer, Berlin,  
875 Heidelberg. doi:10.1007/978-3-642-84379-2.
- 876 Wagner, F. B., Mignardot, J.-B., Goff-Mignardot, C. G. L., Demesmaeker,  
877 R., Komi, S., Capogrosso, M., Rowald, A., Seáñez, I., Caban, M., Piron-  
878 dini, E., Vat, M., McCracken, L. A., Heimgartner, R., Fodor, I., Watrin, A.,  
879 Seguin, P., Paoles, E., Keybus, K. V. D., Eberle, G., Schurch, B., Pralong,  
880 E., Becce, F., Prior, J., Buse, N., Buschman, R., Neufeld, E., Kuster, N.,  
881 Carda, S., von Zitzewitz, J., Delattre, V., Denison, T., Lambert, H., Mi-  
882 nassian, K., Bloch, J., & Courtine, G. (2018). Targeted neurotechnology  
883 restores walking in humans with spinal cord injury. *Nature*, *563*, 65–71.  
884 doi:10.1038/s41586-018-0649-2.
- 885 Wu, L., Wu, Q., Zhang, Q., & Xiong, C. (2017). Electrically induced joint  
886 movement control with iterative learning algorithm. In *2017 2nd International  
887 Conference on Advanced Robotics and Mechatronics (ICARM)*. IEEE. doi:10.  
888 1109/icarm.2017.8273200.
- 889 Xian, B., Dawson, D., de Queiroz, M., & Chen, J. (2003). A continuous asymp-  
890 totic tracking control strategy for uncertain multi-input nonlinear systems. In  
891 *Proceedings of the 2003 IEEE International Symposium on Intelligent Control  
892 ISIC-03*. IEEE. doi:10.1109/isic.2003.1253913.
- 893 Xian, B., Dawson, D. M., de Queiroz, M. S., & Chen, J. (2004). A continuous  
894 asymptotic tracking control strategy for uncertain nonlinear systems. *IEEE*

895 *Transactions on Automatic Control*, 49, 1206–1211. doi:10.1109/TAC.2004.  
896 831148.

897 Yu, H., Huang, S., Chen, G., Pan, Y., & Guo, Z. (2015). Human–robot in-  
898 teraction control of rehabilitation robots with series elastic actuators. *IEEE*  
899 *Transactions on Robotics*, 31, 1089–1100. doi:10.1109/tro.2015.2457314.

900 Yu, H., Huang, S., Chen, G., & Thakor, N. (2013). Control design of a novel  
901 compliant actuator for rehabilitation robots. *Mechatronics*, 23, 1072–1083.  
902 doi:10.1016/j.mechatronics.2013.08.004.

### 903 **Appendix A. Supplementary results**

904 Table A.5 exhibits the fine-tuned gains ( $\alpha_1$ ;  $\alpha_2$ ;  $ks$ ;  $\beta$ ) used for each RISE-  
905 based control-stimulation session and both trajectories. Moreover, Figs. A.10-  
906 A.12 illustrate tracking results on both trajectories and their respective deliv-  
907 ered PWs (Deliv. PWs) for individuals H1 (session  $v$ ), H2 (session  $ii$ ), and H4  
908 (session  $v$ ). Figs. A.13-A.16 compare the results of simulation and real experi-  
909 ments based on empirical tuning or fine-tuned IGA gains. Figs. A.13-A.16 were  
910 selected for illustration purposes only, as the objective here is to highlight the  
911 benefits of using past data for the nonlinear system identification step.

Table A.5: RISE controller gains fine-tuned with IGA used in the experiments with the proposed methodology for both sine and step waves.

Individual	Session	RISE controller gains ( $\alpha_1$ ; $\alpha_2$ ; $ks$ ; $\beta$ )	
		Sine	Step
P1	i	2.61; 3.34; 48.94; 1.78	2.72; 3.57; 47.12; 1.54
P2	i	2.22; 3.54; 39.50; 1.40	3.01; 1.91; 48.34; 2.65
H1	i	3.23; 1.08; 24.74; 5.50	1.37; 1.63; 54.03; 2.36
	ii	1.76; 2.28; 32.30; 2.39	0.64; 1.66; 52.26; 4.00
	iii	3.23; 2.52; 27.33; 2.29	2.30; 4.24; 59.26; 3.49
	iv	2.40; 4.10; 27.05; 2.18	3.12; 5.80; 43.162; 1.35
	v	3.07; 4.37; 21.73; 1.56	2.61; 3.54; 39.50; 1.30
H2	i	1.90; 3.50; 48.00; 3.00	1.90; 3.50; 48.00; 3.00
	ii	1.57; 2.37; 48.45; 1.05	1.38; 1.34; 64.41; 3.72
	iii	1.47; 3.31; 30.01; 1.87	3.54; 3.83; 54.88; 1.92
	iv	1.42; 3.68; 35.09; 1.99	2.07; 1.75; 36.32; 1.96
	v	2.03; 3.02; 36.07; 2.23	2.17; 1.76; 38.53; 1.85
H3	i	1.40; 2.50; 60.00; 3.40	1.47; 2.63; 57.83; 3.36
	ii	2.12; 2.28; 73.74; 1.55	2.77; 3.03; 57.17; 3.47
	iii	4.75; 4.01; 19.56; 2.73	1.56; 3.95; 50.91; 3.05
	iv	0.93; 2.69; 28.09; 2.45	3.22; 3.99; 68.67; 1.26
	v	3.25; 3.45; 22.70; 3.23	2.23; 2.85; 43.33; 2.03
H4	i	1.92; 2.41; 69.71; 1.69	1.92; 2.41; 69.71; 1.69
	ii	1.92; 4.14; 44.26; 1.50	1.92; 2.41; 55.83; 1.69
	iii	3.85; 4.00; 21.51; 2.85	1.22; 1.64; 30.44; 3.50
	iv	1.63; 4.26; 23.74; 1.70	1.03; 6.16; 66.38; 1.14
	v	2.24; 2.22; 28.37; 2.06	2.12; 2.35; 46.93; 1.67
H5	i	3.36; 4.09; 53.19; 3.30	3.65; 1.56; 76.66; 2.69
	ii	2.68; 6.85; 24.64; 3.13	2.84; 1.51; 40.93; 2.54
	iii	3.21; 2.43; 51.30; 3.42	1.16; 2.98; 45.15; 1.20
H6	i	1.52; 2.50; 55.87; 1.67	2.10; 1.08; 51.24; 1.93
	ii	4.89; 4.89; 43.05; 2.36	2.62; 5.22; 25.55; 3.65
H7	i	3.72; 3.85; 45.16; 1.59	2.75; 3.85; 68.51; 1.96
	ii	1.15; 5.96; 44.29; 1.20	2.73; 5.79; 37.57; 2.44

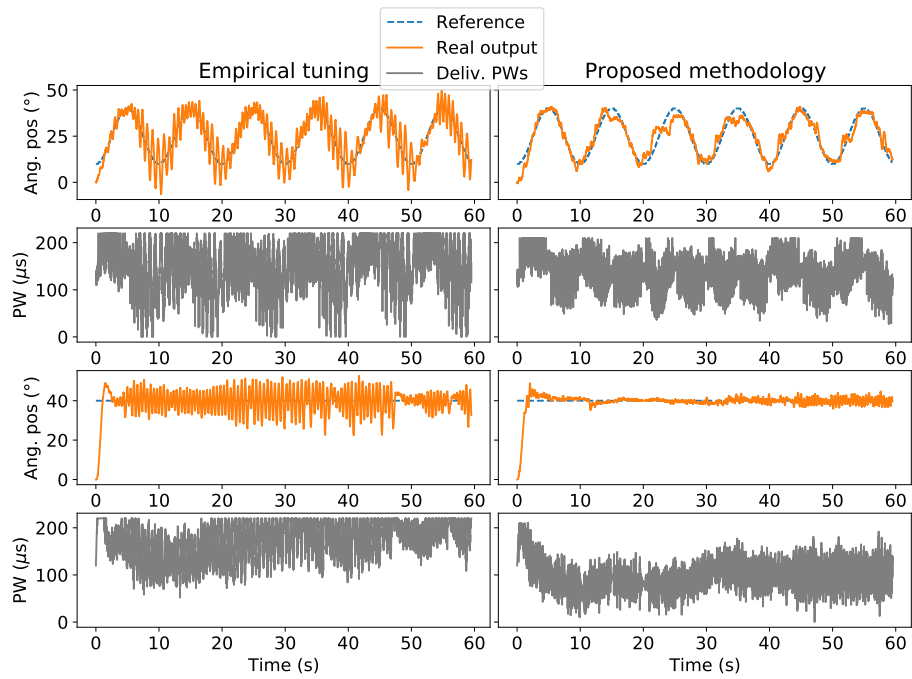


Figure A.10: Experimental results for individual H1 comparing empirical gains and the proposed methodology. The first and second rows illustrate the tracking results for the sine wave and the corresponding delivered PWs, respectively. Similarly, the third and fourth rows illustrate the tracking results for the step wave and the corresponding delivered PWs, respectively.

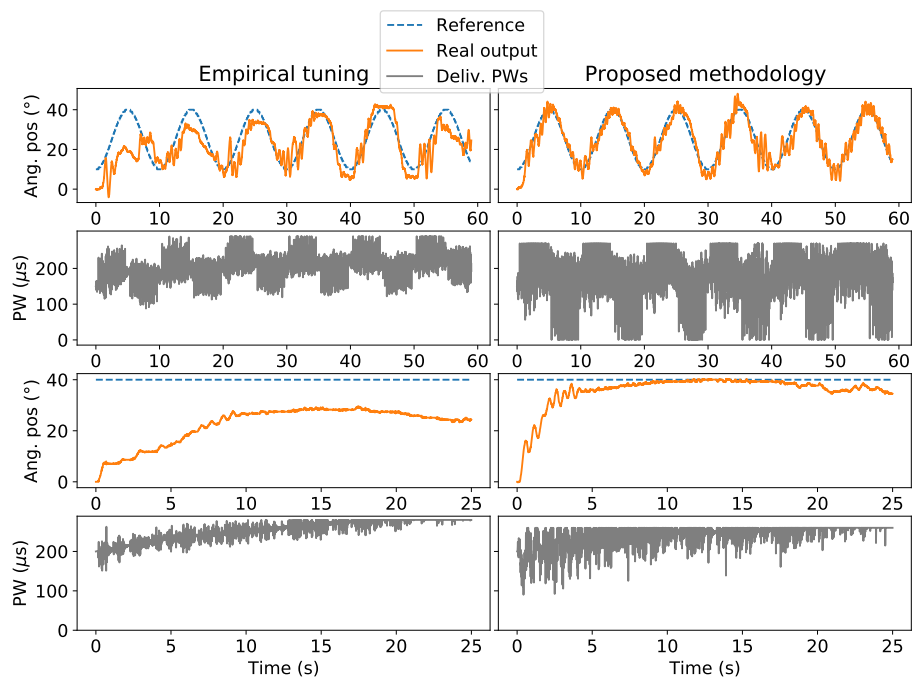


Figure A.11: Experimental results for individual H2 comparing empirical gains and the proposed methodology. The first and second rows illustrate the tracking results for the sine wave and the corresponding delivered PWs, respectively. Similarly, the third and fourth rows illustrate the tracking results for the step wave and the corresponding delivered PWs, respectively.

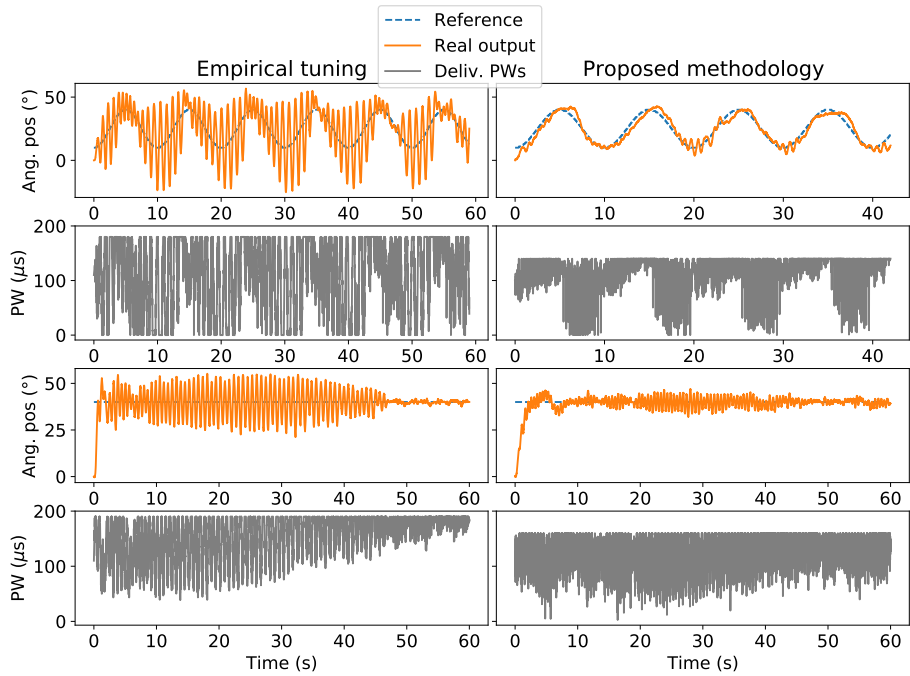


Figure A.12: Experimental results for individual H4 comparing empirical gains and the proposed methodology. The first and second rows illustrate the tracking results for the sine wave and the corresponding delivered PWs, respectively. Similarly, the third and fourth rows illustrate the tracking results for the step wave and the corresponding delivered PWs, respectively.

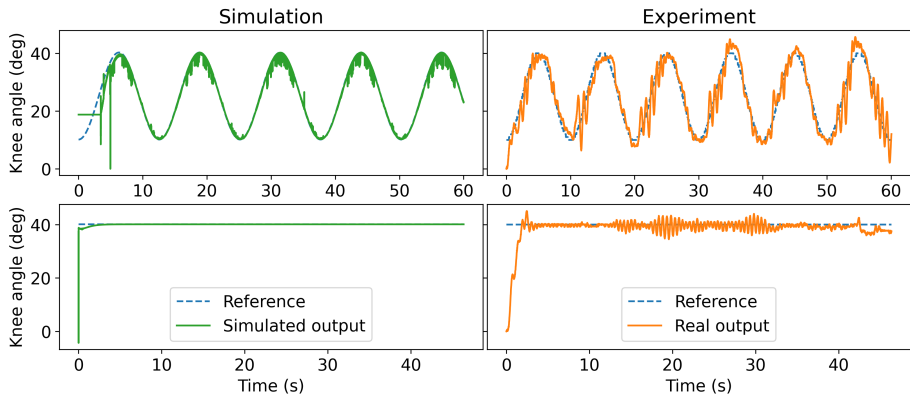


Figure A.13: Comparison of simulation and real experiments for individual H2 using past rehabilitation data to identify the nonlinear model.



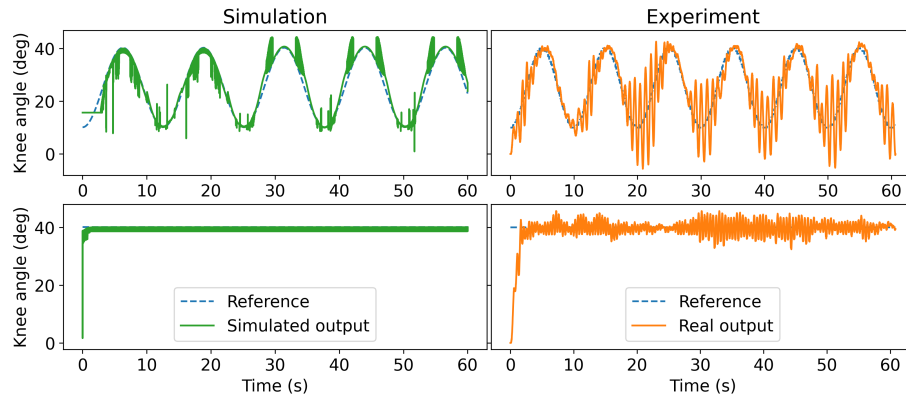


Figure A.14: Comparison of simulation and real experiments for individual H3 using past rehabilitation data to identify the nonlinear model.

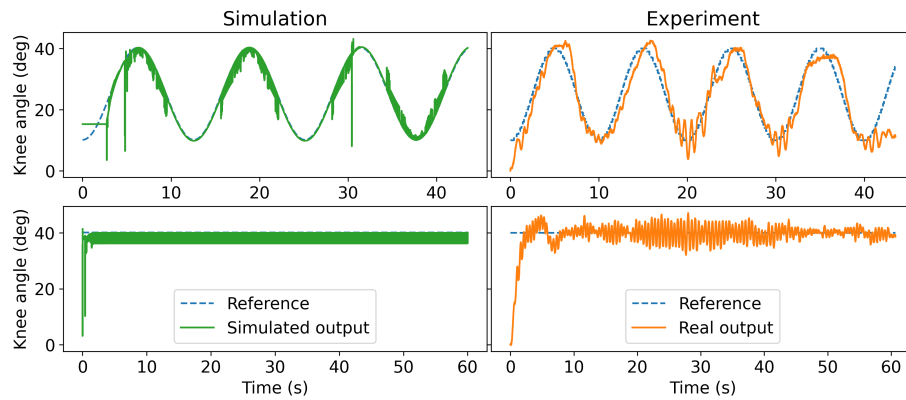


Figure A.15: Comparison of simulation and real experiments for individual H6 using past rehabilitation data to identify the nonlinear model.

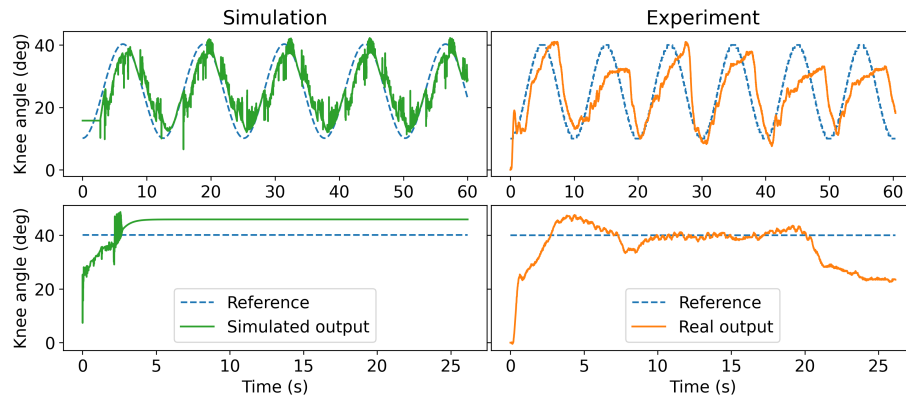


Figure A.16: Comparison of simulation and real experiments for individual H7 using past rehabilitation data to identify the nonlinear model.